ARMY RESEARCH LABORATORY

Exploratory Analysis of Helium Layer Usage for Dynamic Pressure Enhancement in the Large Blast/Thermal Simulator

Stephen J. Schraml

ARL-TR-869

September 1995

NOTICES

REPORT DOCUMENTATION PAGE

Form Approved
OMB No. 0704-0188

1. AGENCY USE ONLY *(Leave blank)*

2. REPORT DATE
September 1995

3. REPORT TYPE AND DATES COVERED
Final, Jan - May 95

4. TITLE AND SUBTITLE
Exploratory Analysis of Helium Layer Usage for Dynamic Pressure Enhancement in the Large Blast/Thermal Simulator

5. FUNDING NUMBERS
4G592-542-U2-203U

6. AUTHOR(S)
Stephen J. Schraml

7. PERFORMING ORGANIZATION NAME(S) AND ADDRESS(ES)
U.S. Army Research Laboratory
ATTN: AMSRL-WT-NC
Aberdeen Proving Ground, MD 21005-5066

8. PERFORMING ORGANIZATION REPORT NUMBER
ARL-TR-869

9. SPONSORING/MONITORING AGENCY NAME(S) AND ADDRESS(ES)

10. SPONSORING/MONITORING AGENCY REPORT NUMBER

11. SUPPLEMENTARY NOTES

12a. DISTRIBUTION/AVAILABILITY STATEMENT
Approved for public release; distribution is unlimited.

12b. DISTRIBUTION CODE

13. ABSTRACT *(Maximum 200 words)*

Numerical simulations of the time-dependent flow in the Large Blast/Thermal Simulator (LB/TS) were executed to model a possible use of that facility for enhancing dynamic pressure using a helium layer positioned on the floor of the expansion tunnel. The simulations were performed using a 2-D, finite difference Euler equation solver with miltiple material models. The flow structure and recorded flow history data for the simulation, employing a single helium layer, are compared to the results of a calculation without a helium layer in order to quantify the dynamic pressure enhancement produced by the presence of the helium layer. The results of the calculations show that the greatest enhancement in dynamic pressure impulse is approximately a factor of two over the case with no helium layer but is limited to a region less than 1 meter from the floor of the expansion tunnel. This limited region of dynamic pressure enhancement is insufficient for blast testing of full-scale military vehicles and equipment.

14. SUBJECT TERMS
blast, blast tubes, flow fields, nuclear weapons, shock tubes, nuclear explosion simulation

15. NUMBER OF PAGES
41

16. PRICE CODE

17. SECURITY CLASSIFICATION OF REPORT	18. SECURITY CLASSIFICATION OF THIS PAGE	19. SECURITY CLASSIFICATION OF ABSTRACT	20. LIMITATION OF ABSTRACT
UNCLASSIFIED	UNCLASSIFIED	UNCLASSIFIED	UL

Intentionally Left Blank

Acknowledgments

The experimental data presented in this report were provided to the U.S. Army Research Laboratory (ARL) by Mr. E. Martinez of the Defense Nuclear Agency. The author appreciates the assistance of Mr. Martinez in providing the data. Thanks also to Bernard Guidos of ARL for providing a technical review of this report and improving the quality of the final manuscript.

Intentionally Left Blank

Table of Contents

Intentionally Left Blank

List of Figures

Intentionally Left Blank

1. Background

Non-ideal blast is a phenomenon associated with the detonation of a nuclear weapon over desert or vegetation-covered land. The detonation of the weapon results in a scenario in which the surface of the earth near the weapon is heated by the fire ball produced during the detonation. The thermally irradiated ground then heats the adjacent air by convection, creating a hot thermal layer of less-than-ambient density and greater-than-ambient sound speed. When the shock wave produced by the detonation reaches the heated air, it is accelerated and weakened because of the increased sound speed of the thermal layer. This acceleration of the flow field causes air of greater density above the thermal layer to be drawn into the accelerated flow field, forming a large wall jet adjacent to the ground.[1] The wall jet is large enough to completely engulf military equipment, exposing it to the high dynamic pressure loading of the non-ideal blast flow.

The phenomenon of non-ideal blast was first observed during nuclear weapons testing at the Nevada Test Site in the 1950s. Many pieces of military equipment that were exposed to blast loading on these desert tests sustained far greater damage than similar equipment experienced in tests in which the weapon was detonated over an ideal surface, such as water. It was found that increased damage to equipment in desert tests was a result of non-ideal blast. The enhanced dynamic pressure associated with this phenomenon significantly increases the aerodynamic drag loading on military equipment and can cause the equipment to experience large displacements. The damage to the equipment comes not from the shock diffraction over the equipment but from the repeated rolling of the equipment across the desert floor.

Because non-ideal blast can inflict severe damage to even shock-hardened equipment, this phenomenon is of great tactical significance. Therefore, to improve the survivability of military equipment in a non-ideal blast environment, the characteristics of the environment must be understood and methods for testing modern equipment must be developed.

2. Ideal and Non-Ideal Blast Environments

The term "ideal" blast refers to the blast environment resulting from the detonation of a nuclear weapon, at an optimized height of burst, over a surface that is perfectly smooth and reflective of blast and thermal radiation. The static and dynamic pressure-time history waveforms resulting from an ideal nuclear blast are characterized by an immediate increase in pressure upon the arrival of the shock front at the observation point, followed by an approximately exponential decay. As an example, Figure 1 represents the static and dynamic pressure histories that would be observed at a point 927 m from ground zero of a 32 kT weapon detonated over an ideal surface.

In reality, no surface exactly qualifies as ideal. However, a blast environment can be considered ideal if the effects of the surface characteristics have a minimal influence on the

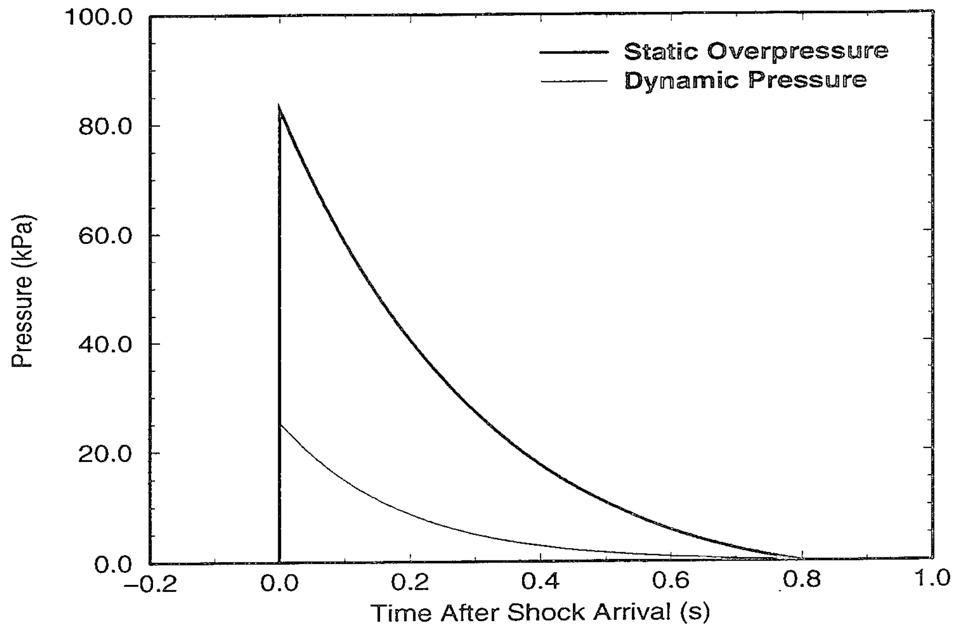

Figure 1. Ideal Pressure-Time Histories from 32 kT Weapon

resulting blast. If surface characteristics play a significant role in the development of the blast environment, then the blast environment is referred to as "non-ideal".

Because there can be a large number of combinations of surface characteristics that can cause a blast environment to be non-ideal, it is impossible to identify a single type of waveform and label it as the non-ideal blast wave. However, within the context of damage to tactical military equipment, we will limit the definition of non-ideal blast to that which results from flow field acceleration because of the presence of a thermal layer. The dynamic pressure, p_d, of a fluid in motion is defined in Equation 1 as

$$p_d = \frac{1}{2}\rho U^2 \tag{1}$$

in which ρ is the density and U is the velocity.[2]

Because of the acceleration of the flow field caused by the presence of the thermal layer, and the entrainment of dense air into the resulting wall jet, the dynamic pressure produced by the non-ideal blast phenomenon is significantly greater than that of the ideal case. This is illustrated in Figure 2, which is a comparison of ideal[3] and non-ideal static and dynamic pressure waveforms.

Figure 2 illustrates several key characteristics of this type of non-ideal blast event:

1. The time of arrival of the shock wave at the observation point is earlier in the non-ideal case than in the ideal case. This is a direct result of the acceleration of the shock front because of the presence of the thermal layer of greater sound speed.

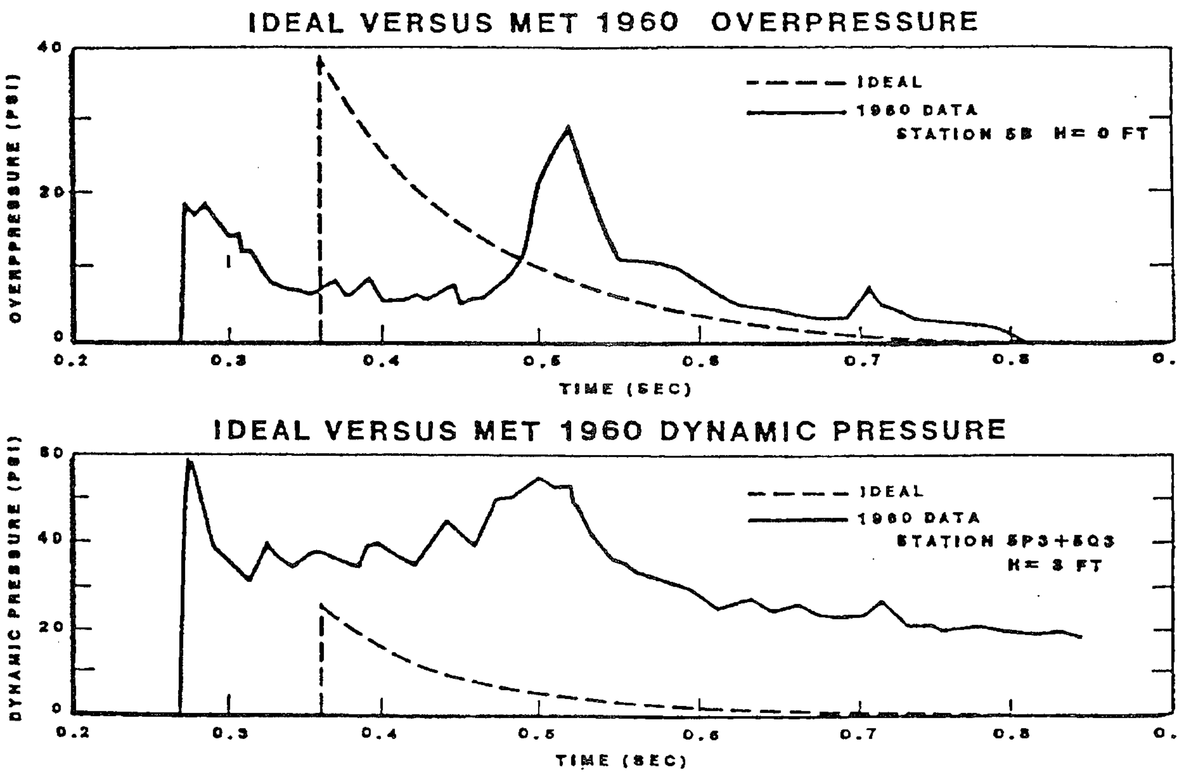

Figure 2. Comparison of Ideal and Non-Ideal Waveforms

2. The amplitude of the incident static overpressure of the non-ideal wave is less than that of the ideal case. As a result, a thermally "precursed," non-ideal blast will produce a reduced level of damage to a target because of shock diffraction.

3. The dynamic pressure produced by the non-ideal blast event is, at all times in the pressure history, greater than the dynamic pressure produced by the detonation of the same weapon over an ideal surface. Consequently, the dynamic pressure impulse (the area under the dynamic pressure history curve) for the non-ideal case will be several times greater than the ideal dynamic pressure impulse. The dynamic pressure impulse is an indicator of the amount of energy delivered to the target that will contribute to whole body response. Because non-ideal blast can produce dynamic pressure impulses that are many times greater than the equivalent ideal event, military equipment that is hardened to survive in an ideal blast environment may experience damage or destruction by displacement in a non-ideal blast scenario.

Dynamic pressure measurements from the nuclear weapon test MET can be compared to the equivalent ideal blast environment illustrated in Figure 1 to determine the dynamic pressure impulse enhancement for that particular weapon and range to target.[3] By scaling the data from MET to the 32 kT, 927 m ideal conditions, the ratio of actual (non-ideal) to ideal dynamic pressure impulse can be obtained. This ratio is calculated to be approximately 3.5.

Another nuclear weapon test, PRISCILLA, has been simulated with the second order, hydrodynamic, advanced research code (SHARC) to model the non-ideal blast environment produced by the interaction of the blast wave with the heated layer created by the thermal radiation of the desert surface.[4] The results of this work indicate that the dynamic pressure impulse produced by the detonation of a 36.6 kT weapon over a desert surface will be approximately six times greater than the dynamic pressure impulse of the equivalent ideal event at a ground range of 970 m to the target.

3. Simulation of Non-Ideal Blast with Shock Tubes

The ban on above-ground nuclear testing has forced the military to develop alternate methods for testing vehicles and equipment to the effects produced by nuclear weapons. Blast testing of military equipment is typically accomplished through either the detonation of high explosives (HE) or the use of specially configured shock tubes. Tests involving HE are typically limited to very small explosive yields, approximately several kilotons.

Larger weapon yields through the tactical range may be simulated in shock tubes, which are referred to as large blast simulators. These blast simulators consist of a driver system that typically contains compressed air or nitrogen gas. The driver system feeds into an expansion tunnel that contains a test section where the target is placed for a test. The driver gas is initially separated from the ambient expansion tunnel gas by a thin diaphragm. When the diaphragm is ruptured, the compressed driver gas exits the driver and enters the expansion tunnel, forming a shock wave. Through careful design of the driver and expansion tunnel geometry, and selection of appropriate driver gas initial conditions, these blast simulators are capable of producing high fidelity simulations of ideal nuclear blast waves.

The facility of interest here is the Large Blast/Thermal Simulator (LB/TS) located at the White Sands Missile Range in New Mexico. The LB/TS is a blast simulator capable of producing ideal blast waveforms with incident static overpressures of 14 kPa to 240 kPa at simulated nuclear weapon yields of 1 kT to 600 kT.[5]

The driver system of the LB/TS consists of nine cylindrical drivers, which feed into a half-cylinder expansion section. Each driver has an interior diameter of 1.83 m. The volume of each driver can be adjusted, and the maximum available volume of all nine drivers is 583 m^3. The downstream ends of the drivers converge to an interior diameter of 0.91 m and end at a double diaphragm system. The expansion section has a nominal diameter of 20 m, with a cross-sectional area of 163 m^2. The expansion section is 170 m long, with the test section located 101 m from the upstream end of the expansion section. Throughout this report, the upstream end of the expansion section refers to the beginning of the half-cylinder tunnel.

At the downstream end of the expansion section is an active rarefaction wave eliminator (RWE). The RWE is a device that modifies the flow exiting the expansion section in such a way as to minimize flow disturbances that originate when the shock wave exits the expansion section.[6] Such disturbances destroy the fidelity of an ideal blast simulation and therefore must be reduced or eliminated to properly simulate the ideal nuclear blast environment.

The recent interest in the threat of the non-ideal blast phenomenon to system survivability has generated a requirement to simulate non-ideal blast waveforms within the expected operational range of many Army vehicles and systems. The non-ideal blast phenomenon has been successfully simulated on full-scale military equipment using a helium layer on the ground during HE tests.[7] The helium layer has a greater sound speed and lower density than the ambient air and consequently produces the same acceleration effect as the heated thermal layer in the actual nuclear blast event.

The high cost and low explosive yields of HE testing make them impractical for testing the survivability of a large number of systems to the non-ideal blast environment. For this reason, it would be advantageous to configure the LB/TS for non-ideal blast testing. There are several possible methods in which the LB/TS could be employed to produce the high dynamic pressure associated with non-ideal blast, the most notable of which are

1. Controlled, staggered firing of drivers, combined with modified RWE closing functions.
2. Removal of the RWE from the expansion tunnel of the LB/TS and testing the vehicle outside the expansion tunnel in the exit jet of the shock tube.
3. Use of a helium layer inside the expansion tunnel to reproduce the flow field acceleration phenomenon employed in non-ideal blast HE tests.
4. Combinations of the previous three items.

This report documents a computational study to estimate the effectiveness of helium layers as a means of producing a high dynamic pressure blast environment in the LB/TS.

4. Development and Validation of the Numerical Model

The U.S. Army Research Laboratory (ARL) employs a number of flow solvers for modeling blast flows. The solver that is selected for a given problem is one best suited to the physics of the phenomenology being considered. For the analysis described in this report, the SHARC code was selected. SHARC is a family of codes centered around a two-dimensional (2-D)/three-dimensional (3-D), explicit, finite difference, Eulerian hydrocode.[8] It is capable of solving flows with multiple materials and supports a $k-\epsilon$ turbulence model.[9] SHARC has been heavily used in the simulation of blast and has been validated for simulating time-dependent flow in shock tubes.[10]

The LB/TS, with its nine drivers feeding into a single, semi-cylindrical expansion section, is a geometrically 3-D facility. However, the large cost of 3-D hydrocode calculations makes them impractical for this type of initial, exploratory analysis. As a result, trade-offs need to be made so that the 3-D facility can be simplified into a 2-D representation and still preserve the dominant flow characteristics of the actual facility. This is accomplished by "lumping" together all cross-sectional flow areas at every point along the length of the shock tube. In the case of the nine drivers of the LB/TS, a 2-D computational model will contain a single driver with the equivalent volume and cross-sectional area of all nine LB/TS drivers. This lumped driver will then feed into an expansion section with a cross-sectional area that is equivalent to that of the LB/TS.[11]

For most LB/TS calculations, an axisymmetric model is employed, reducing the facility to a shock tube with a single cylindrical driver connected to a cylindrical expansion section by a converging nozzle and cylindrical throat. However, for the case in which a helium layer is placed on the floor of the LB/TS, it would be incorrect to model this configuration with an axisymmetric model. Consequently, a 2-D Cartesian model was developed to model the interaction of the primary blast flow with the helium layer. This type of model is sometimes referred to as having "planar" symmetry because the computational domain represents a single plane in a 3-D space which has a unit depth perpendicular to that domain.

As stated earlier, the expansion section of the LB/TS is that of a half-cylinder with a diameter of 20 m and a cross-sectional area of 163 m^2. Therefore, the unit depth of the planar model is 20 m. Preserving the cross-sectional area of the expansion section in the planar model results in an expansion section height of 163.18 $m^2/20\ m = 8.16\ m$. The geometry of the lumped driver system was derived in a similar manner. The resulting 2-D Cartesian model is illustrated in Figure 3. This geometry was discretized into the computational domain using a mesh of 950 grid points in the longitudinal direction and 110 grid points in the vertical direction. The minimum cell width used in the grid was 7.4 cm, with an aspect ratio close to 1 in the regions of interest.

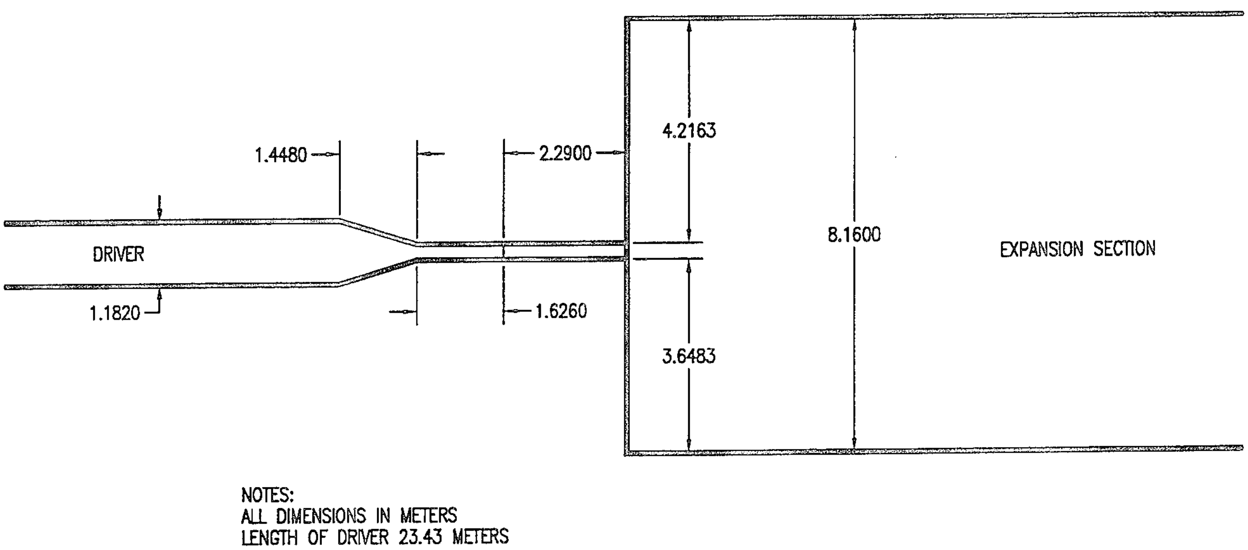

Figure 3. 2-D Cartesian, Lumped Area Model of LB/TS

Before a helium layer calculation was run, it was necessary to use the model to simulate an LB/TS test with no helium layer in order to validate the model. At the time of the model development, only one test had been performed in the LB/TS using all nine driver tubes. This test had been performed using a driver overpressure of 3.45 MPa, a driver gas temperature of 415 K, and the maximum available driver volume. This test resulted in a high fidelity simulation of an ideal blast from a 32 kT weapon. The incident static overpressure of this experiment was approximately 85 kPa. The quality and availability of this set of LB/TS test data[12] make it attractive to the type of analysis described in this report.

The SHARC Cartesian model was executed using the driver conditions from the LB/TS experiment. Time history data from the calculation were collected at sets of data-gathering stations positioned along the length of the expansion section, 30 m, 60 m, 90 m, 101.5 m, 120 m, 150 m from the upstream end of the expansion section. At each of these longitudinal positions, individual stations were placed vertically at 0 m, 1 m, 2 m, 3 m, 4 m, 6 m, and 8 m from the floor of the expansion section. The longitudinal station position of 101.5 m corresponds to the location of test section in the expansion tunnel of the LB/TS. Therefore, the primary flow field measurements were taken at this location. The static overpressure from the LB/TS experiment is compared to that of the SHARC calculation in Figure 4, while the dynamic pressure history comparison is shown in Figure 5. In these figures, the time corresponding to $t = 0.0\ s$ is the arrival of the incident shock wave at the 101.5 m test section.

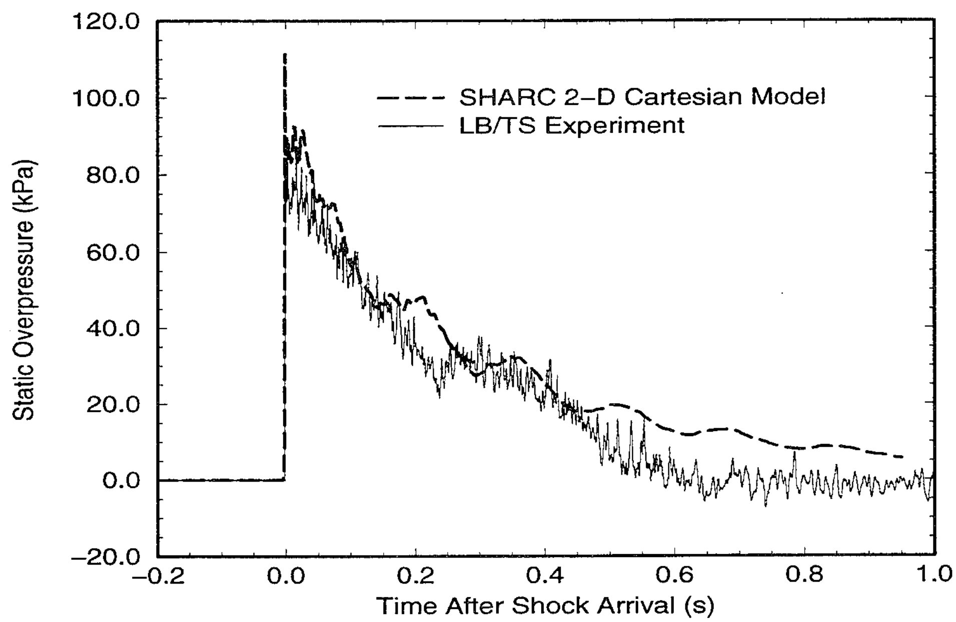

Figure 4. Static Overpressure Histories at 101.5 m

Figure 4 shows that the SHARC model overpredicts the measured strength of the incident shock at $t = 0.0\ s$. As the pressure history decays, the calculated static overpressure is mostly within the scatter of the data or about 5 kPa to 10 kPa higher than the data.

Figure 5 shows that the SHARC model also overpredicts the incident dynamic pressure at $t = 0.0\ s$. As the pressure history decays, the calculated dynamic pressure is typically within 5 kPa to 7 kPa from the measured data. For $t < 0.3\ s$, the calculated dynamic

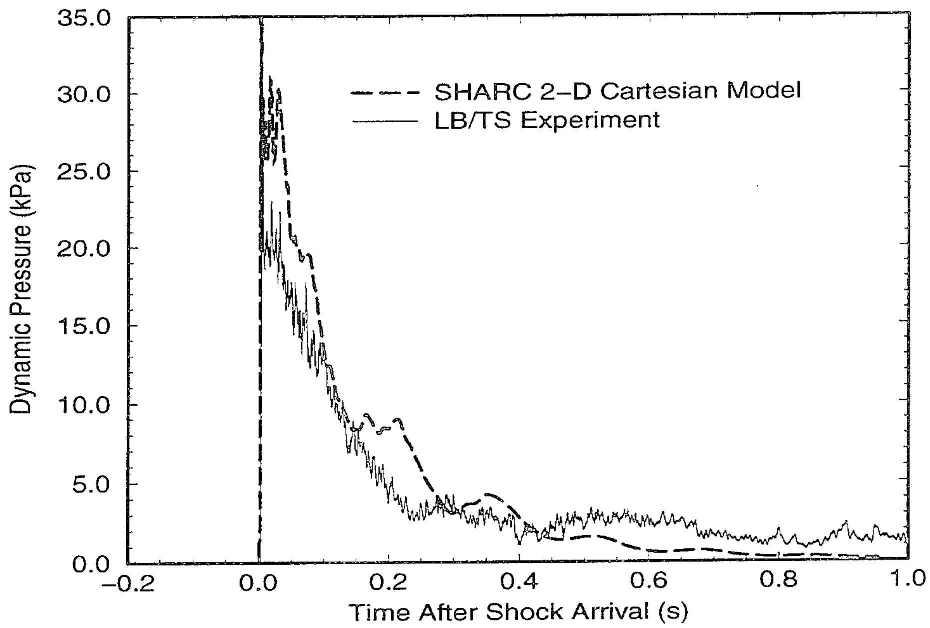

Figure 5. Dynamic Pressure Histories at 101.5 m

pressure is higher than the measured pressure; for $t > 0.3\ s$, the opposite is true. Using these pressure histories, the calculated dynamic pressure impulse at the 101.5 m station is 4.33 $kPa{\cdot}s$, and the measured value is 4.54 $kPa{\cdot}s$, a difference of 4.8%.

This comparison of the LB/TS experiment to the SHARC calculation validates the 2-D Cartesian model for simulating the blast wave formation and evolution in the LB/TS. With the model validated, it was then used to simulate a hypothetical experiment in which a helium layer was positioned in the expansion section of the LB/TS. The enhancement in dynamic pressure impulse above the 4.54 $kPa{\cdot}s$ produced by the calculation will be the primary benchmark by which the performance of the helium layer will be determined.

5. Configuration of the Helium Layer

In configuring a helium layer for a shock tube experiment, it is necessary to consider the effects of the helium layer on the shock wave dynamics in the expansion tunnel. Experience from HE tests with helium layers indicates that a significant run length of helium layer is needed upstream from the target to create a proper non-ideal blast simulation.[13] However, maximizing the length of the helium layer upstream from the target in a shock tube will minimize the useful duration of the non-ideal blast simulation because of the interaction of reflections from the roof of the expansion tunnel. The height of the wall jet produced by the acceleration of the flow because of the presence of the helium layer is influenced by the thickness of the helium layer itself. Unfortunately, a layer that is excessively thick will reduce the time for disturbances that originate at the top of the layer to reach the roof of the expansion tunnel and again destroy the fidelity of the simulation. Too thick a layer will also fail to produce the oblique precursor and the shear layer off the triple point, with no rotation and no wall jet being produced.

Based on these considerations, it was decided that, for this exploratory analysis, a helium layer 30 m long and 22 cm thick would provide an acceptable compromise between creation of a non-ideal blast waveform and the influence of the reflected waves originating at the walls and roof of the expansion section. The helium layer was positioned longitudinally in the expansion section so that there was a 21.5 m length of layer upstream from the test section and 8.5 m downstream from the 101.5 m test section.

6. Results of the Helium Layer Simulation

The SHARC simulation of the helium layer configuration was executed using the $k - \epsilon$ turbulence model and required 100 CPU hours to reach 550 ms of simulation time on a Silicon Graphics R4400 workstation. This amount of simulation time was not enough to complete the positive phase of the blast at the test section but was sufficient to determine the effectiveness of the helium layer in producing a non-ideal blast environment.

6.1. Station Data Analysis

The initial analysis of the results of the helium layer calculation was performed by studying the pressure-time histories recorded at the 101.5 m stations and comparing them to the results of the calculation with no helium layer. The first station data examined were from the station 2 m from the floor of the expansion section. This station is considered to be one of the most important because it is located in the test section of the LB/TS and the 2 m vertical height from the floor is approximately in the center of many trucks and other vehicles which will be tested in the LB/TS. The static overpressures at this station are illustrated in Figure 6, comparing the result of the helium layer calculation with the result of the calculation with no helium layer.

The result of the calculation with no helium layer shows the ideal blast waveform that is produced by the LB/TS. It is characterized by the instantaneous increase in pressure upon the arrival of the shock front at the station, followed by an approximately exponential decay in pressure. The helium layer calculation produced a static overpressure at this station that has some of the qualities of the "classic" non-ideal static overpressure waveform illustrated in Figure 2 but on a much reduced scale. The shock arrives at the station only a few milliseconds earlier than that of the ideal case.

Figure 7 shows the dynamic pressure histories from the same station. Except for the slight differences between the histories immediately following the shock arrival, the two results are nearly the same. In particular, there is no increase in the dynamic pressure resulting from the presence of the helium layer at this station.

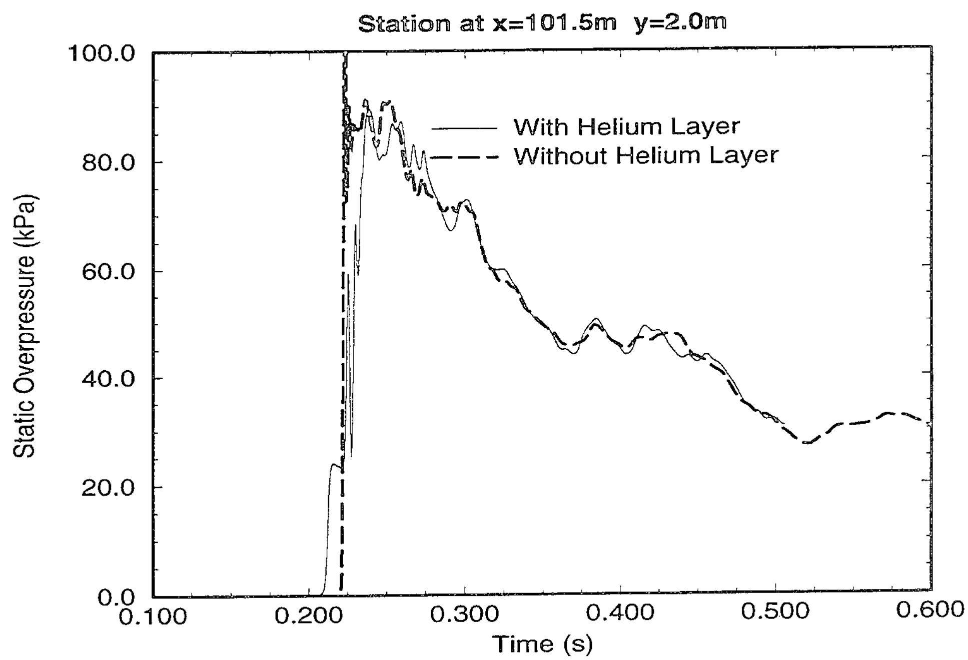

Figure 6. Static Overpressure Histories at Test Section, 2 m from Floor

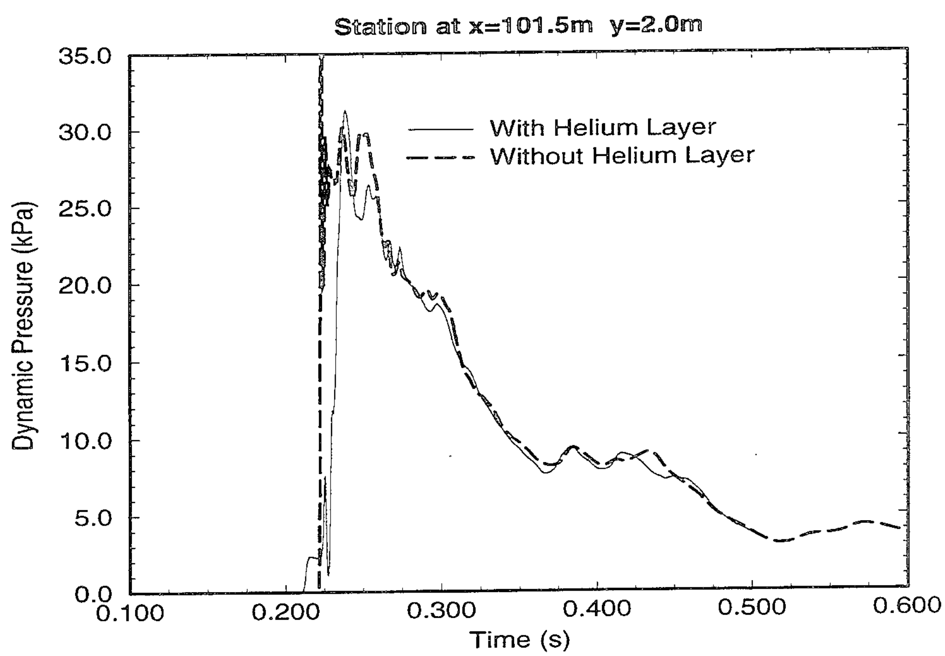

Figure 7. Dynamic Pressure Histories at Test Section, 2 m from Floor

The next pressure-time history data examined were from the station positioned on the floor of the expansion section, at the same 101.5 m longitudinal position. The dynamic pressure histories produced by the two calculations are illustrated in Figure 8. This figure shows that the presence of the helium layer produces a significant increase in the dynamic pressure immediately following the arrival of the precursed shock front. This period of increased dynamic pressure has a duration of less than 50 ms. After this period of increased dynamic pressure, the contribution of the helium layer disappears, and the result of the helium layer calculation practically coincides with the calculation that had no helium layer.

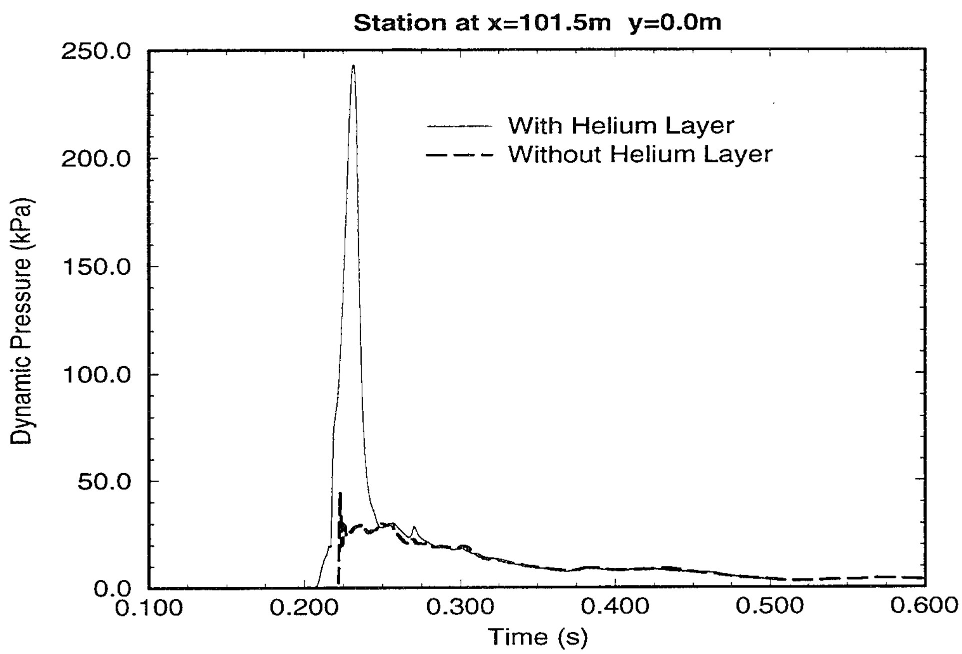

Figure 8. Dynamic Pressure Histories at Test Section, on Floor

The dynamic pressure impulse histories for all stations at the 101.5 m position are presented in Figure 9. This figure clearly illustrates that the increase in dynamic pressure impulse that results from the presence of the helium layer is noticeable only on the floor of the expansion section. The curves show that the dynamic pressure impulse for the 0 m high station is, at all times, greater than that of the other vertical positions and that the other vertical positions are nearly identical.

As stated earlier in this report, the primary purpose of the helium layer is to produce a simulation of a thermally precursed, non-ideal blast wave, with particular emphasis on the dynamic pressure impulse over ideal blast waveforms. The effectiveness of the helium layer in enhancing the dynamic pressure can be determined by calculating the ratio of the dynamic pressure impulse from the helium layer calculation to that with no helium layer. This was done for the data collected at the 101.5 m stations and provided in Figure 10. This figure shows a profile of the ratio of the dynamic pressures as a function of the height of the station from the floor of the expansion section. The dashed line represents a value

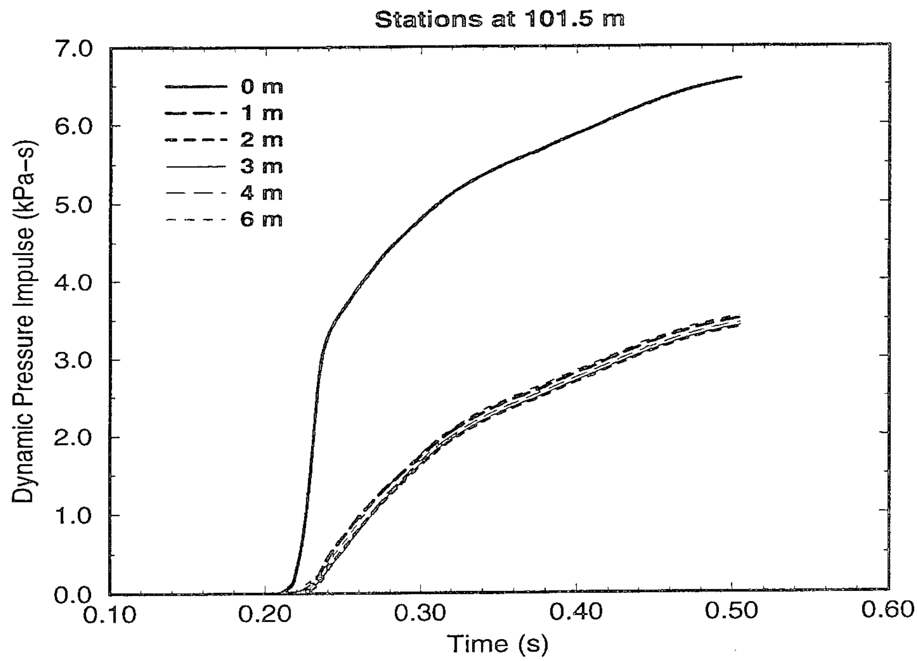

Figure 9. Dynamic Pressure Impulse Histories at Test Section

of unity for the calculation with no helium layer. This line also serves as a reference in determining the effectiveness of the helium layer data, which are represented by the solid line with square markers. This curve further illustrates the finding that the dynamic pressure impulse enhancement resulting from the helium layer is only noticeable on the floor of the expansion section. Here, the dynamic pressure from the helium layer calculation is nearly 1.8 times greater than the result from the same station in the calculation with no helium layer. However, the data collected at the stations above the surface of the floor show that the dynamic pressure impulse at these stations is actually slightly less for the helium layer calculation than for the calculation with no helium layer.

Because the helium layer failed to produce the desired non-ideal blast environment at the test section of the LB/TS, dynamic pressure histories at other longitudinal positions were examined. Figure 11 shows the data gathered on the floor of the expansion sections at longitudinal positions of 90 m, 101.5 m, and 120 m. In the calculations, data-gathering stations were placed at longitudinal positions upstream from the 90 m station, but because the helium layer began at 80 m, there was no influence of the helium layer at these stations. There was also a vertical set of stations at a position 150 m from the upstream end of the test section, but this location is so close to the downstream end of the LB/TS expansion section, that testing of equipment is not likely there.

Figure 11 shows that the dynamic pressure histories on the floor of the expansion section at 90 m and 101.5 m are very similar, with the duration of the period of increased dynamic pressure slightly greater for the 101.5 m station. Of the three traces in the figure, the dynamic pressure history for the station at 120 m shows the most promise of creating the

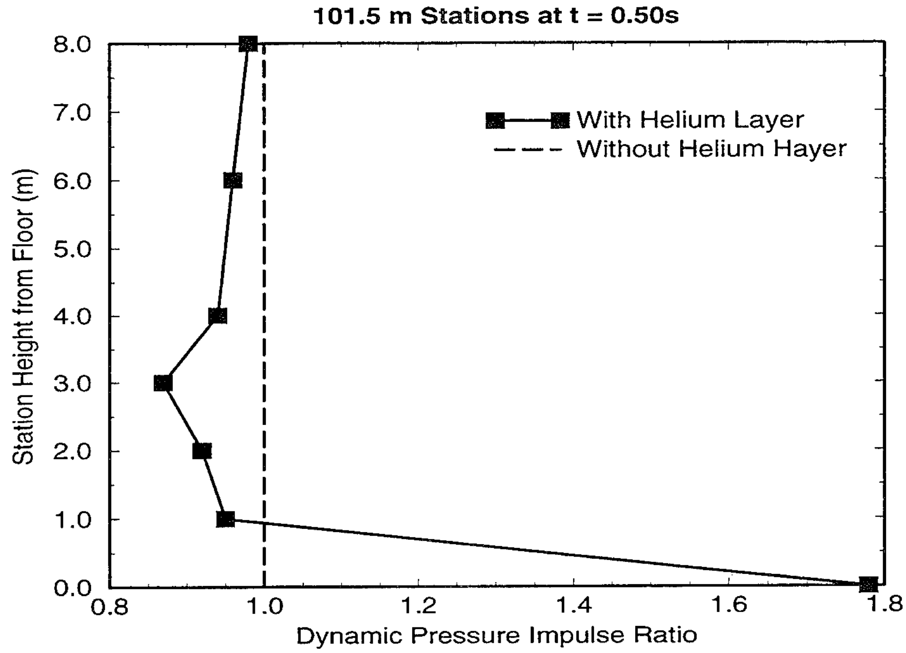

Figure 10. Dynamic Pressure Impulse Enhancement at Test Section, 500 *ms*

type of waveform illustrated in Figure 2. This history shows that, while the dynamic pressure level is not as high as that at the other longitudinal positions, the duration of the increased dynamic pressure is 70 *ms*.

In Figure 12, the dynamic pressure impulse histories are plotted for all the vertical stations at the 120 *m* longitudinal position, in the same manner used for the 101.5 *m* position in Figure 9. This figure shows that the variation in dynamic pressure impulse has a greater vertical distribution than at the 101.5 *m* position.

Finally, the dynamic pressure impulse enhancement at the 120 *m* position is determined by again illustrating the ratio of dynamic pressure impulse for the two calculations as a function of the vertical position of the stations. Figure 13 again shows the result from the calculation with no helium layer represented by a value of unity for all vertical positions. The helium layer result at this longitudinal position illustrates that the dynamic pressure impulse is greater than that with no helium layer up to about 2 *m* from the floor. However, the enhancement in dynamic pressure impulse is minimal at these positions, with the maximum occurring at the floor at only 1.3 times that of the calculation with no helium layer. For stations above a vertical position of 2 *m*, the dynamic pressure impulse produced by the presence of the helium layer was again less than the case in which no helium layer was used. This result and the result of Figure 10 clearly show that the use of a helium layer in the LB/TS will produce highly non-uniform dynamic pressure loading of test articles.

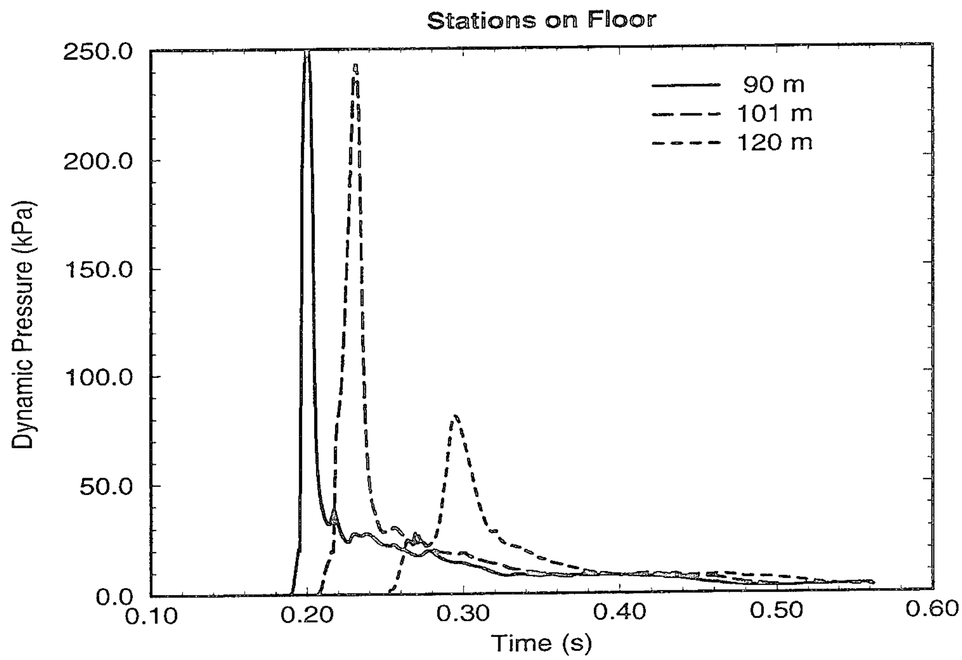

Figure 11. Dynamic Pressure Histories on Floor

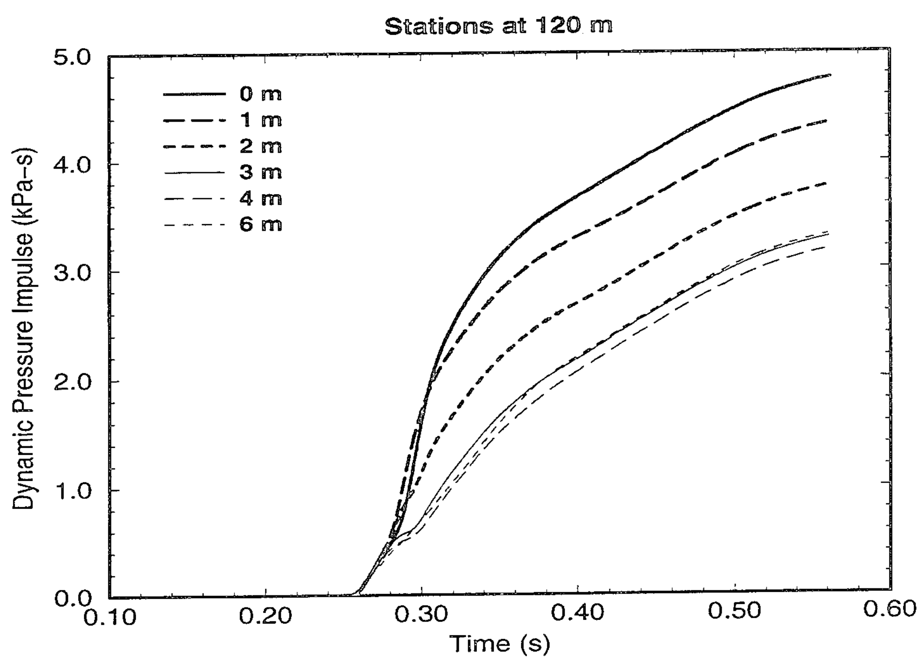

Figure 12. Dynamic Pressure Impulse Histories at 120 m

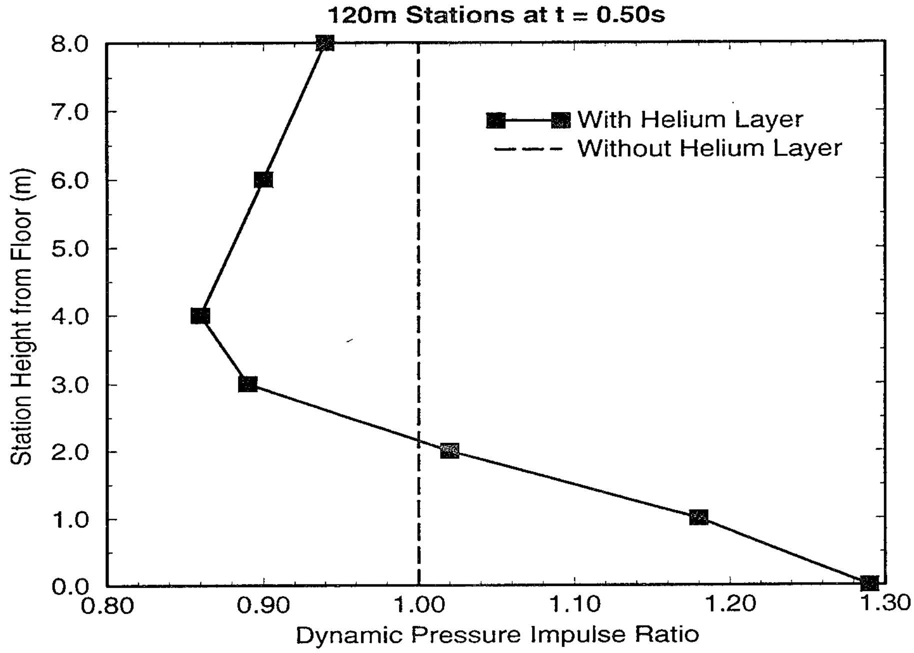

Figure 13. Dynamic Pressure Impulse Enhancement at 120 m, 500 ms

6.2. Flow Field Analysis

Significant insight into the dynamics of the flow can be obtained by analyzing of flow field data, which are saved at regular intervals during the calculations. In the following figures, the dynamic pressure in the expansion section of the LB/TS is shown for the calculations with and without the presence of the helium layer for instants in time of 200 ms, 300 ms, and 400 ms. In these figures, only the portion of the expansion section from longitudinal positions of 75 m to 150 m is shown. The dynamic pressure in all figures is plotted to the same linear scale in which the maximum is 30 kPa and the minimum is 0 kPa. Any value in the plotted region with a dynamic pressure greater than 30 kPa is represented by magenta, the color that corresponds to precisely the maximum value in the legend.

Figures 14 and 15 represent dynamic pressure from the two calculations at 200 ms. Figure 14 shows the planar shock front of the case with no helium layer located at about 90 m from the upstream end of the expansion section. Figure 15 clearly shows the development of the precursor with a region of high dynamic pressure at the floor beginning to accelerate ahead of the primary shock.

At 300 ms, the shock front is located approximately 140 m from the upstream end of the expansion section. As illustrated in Figures 16 and 17, at this point in time, there is no visible influence of the helium layer on the shape of the shock front. Close to the floor, at a longitudinal position of 120 m, exists a region of high dynamic pressure, which confirms the findings of Figure 11. At the test section, 101.5 m from the beginning of the expansion section, the dynamic pressure levels are the same for the two calculations.

Figures 18 and 19 show the results of the two calculations at 400 ms. By this time, the shock front has exited the expansion tunnel. The flow field plots for the two calculations show almost no difference between the dynamic pressure levels throughout most of the expansion section.

The effect of the blast wave on the helium layer can be examined by plotting the density of helium in the expansion section at several times during which the solution was saved. In a manner similar to the dynamic pressure flow field plots, Figures 20 through 23 show the helium density plotted in a common linear scale between a minimum of 0.00 kg/m^3 and a maximum of 0.25 kg/m^3. The solution at 150 ms is provided in Figure 20. At this time, the shock front has not yet reached the upstream end of the helium layer. The undisturbed helium layer can be clearly seen in the region of magenta extending from 80 m to 110 m longitudinally in the expansion section.

At 200 ms, the incident shock has encountered the upstream end of the helium layer in Figure 21. The density levels in the helium layer show that the blast wave is compressing the helium and beginning to drive the upstream end of the layer toward the downstream end. This compression of the layer is further illustrated in Figure 22, a solution at 250 ms. Finally, by 300 ms, the layer is lifted off the floor of the expansion section and carried downstream by the primary flow within the expansion section, as shown in Figure 23.

Combining the pressure-time history data with the information available in the flow field solutions, it is clear that the helium layer is only effective in producing enhanced dynamic pressure at the test section, while it is present at the test section. Even then, this region of enhanced dynamic pressure is isolated to a region within the layer itself. At the time that the blast wave compresses the helium layer to the point where it is no longer present at the test section, the dynamic pressure enhancement ceases and the dynamic pressure waveform coincides with that produced by a simulation with no helium layer.

7. Summary

The recent interest in non-ideal blast effects in the tactical regime has generated a requirement to test military equipment in a simulated, non-ideal blast environment. The purpose of this testing requirement is to determine the severity of the non-ideal blast threat to military equipment. There is presently no specification that requires military equipment to survive in the non-ideal blast environment. The most distinguishing feature of non-ideal blast is the significant increase in dynamic pressure as compared to blast over a perfectly smooth, energy reflecting surface.

Use of the recently constructed LB/TS is one possibility of satisfying this test requirement. To create the high dynamic pressure, non-ideal blast environment, it will be necessary to modify the configuration and operation of the LB/TS. The placement of a helium layer on the floor of the LB/TS has been suggested as a means of accomplishing this task.

This report described an exploratory analysis in which the interaction of the primary blast flow with the helium layer was modeled using SHARC. The analysis shows that the greatest dynamic pressure impulse enhancement produced by the LB/TS helium layer calculation was less than a factor of 1.8 and was limited to a region within 1 m to 2 m from the floor of the expansion section. The dynamic pressure impulse above that region was actually less than that produced by the simulation with no helium layer. The profile of dynamic pressure impulse as a function of height at the 101.5 m and 120 m longitudinal positions showed a large vertical gradient. This would ultimately result in nonuniform dynamic pressure loading of test articles and would significantly limit the fidelity of the test.

Analysis and simulation of actual nuclear testing has revealed that, for the blast environment studied here, dynamic pressure impulse enhancement of about 3.5 to 6 can be expected from the detonation of a tactical nuclear weapon over a desert surface. In order for the LB/TS to become an effective non-ideal blast simulation facility, it must be capable of replicating this type of dynamic pressure environment. The exploratory analysis presented in this report indicates that the use of helium layers alone will not be sufficient to perform this task.

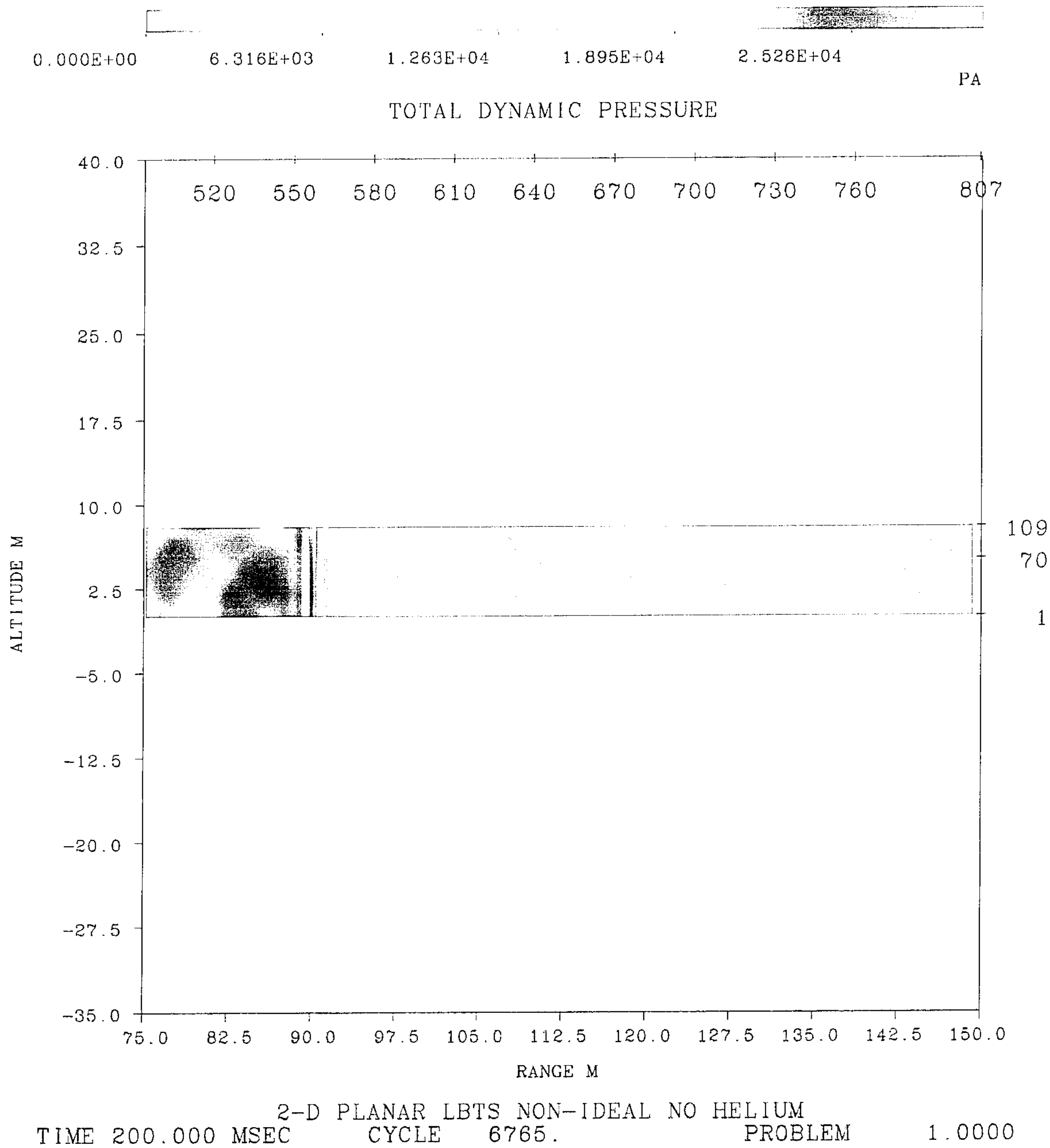

Figure 14. Dynamic Pressure in Expansion Section at 200 ms without Helium Layer

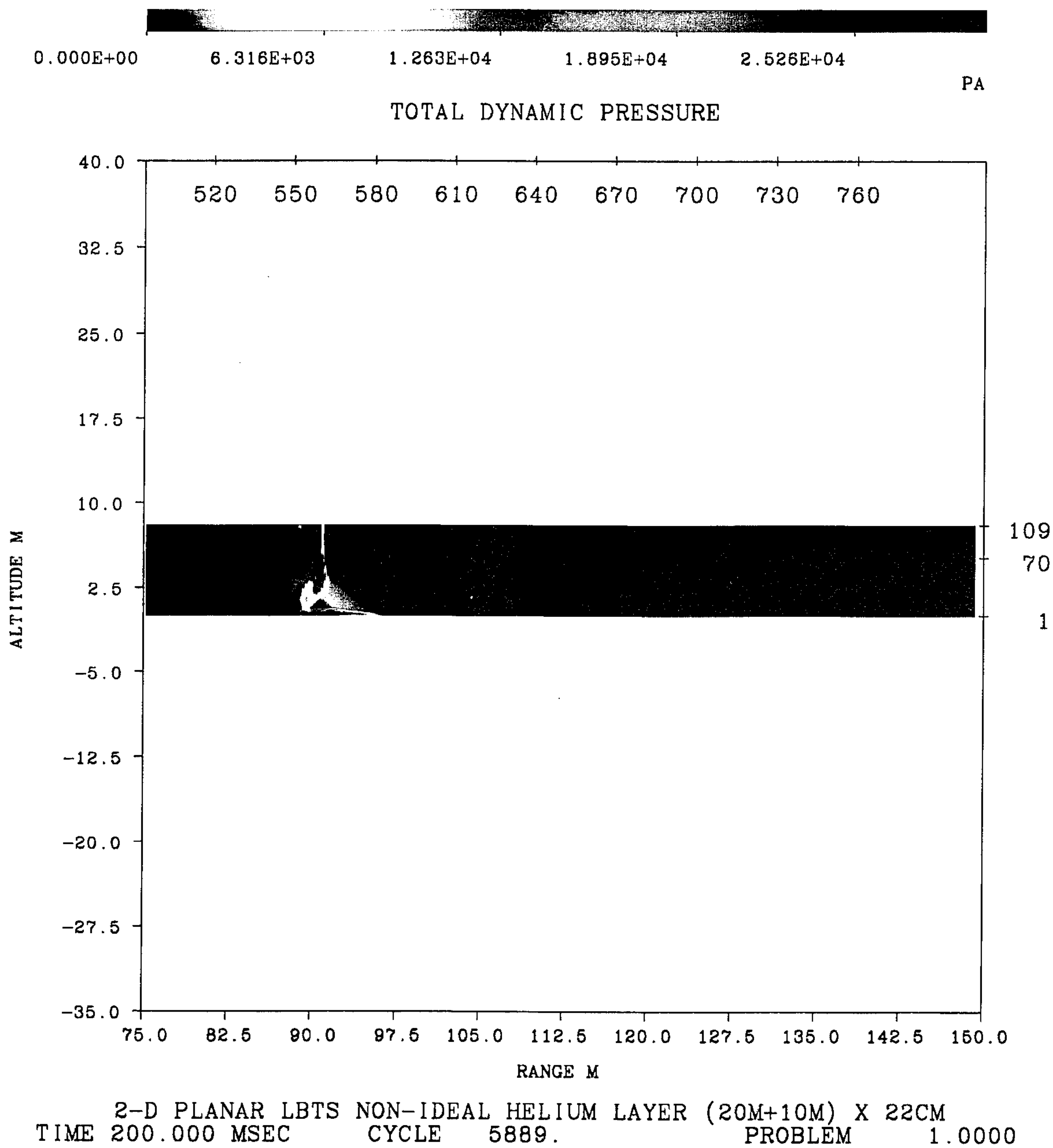

Figure 15. Dynamic Pressure in Expansion Section at 200 ms with Helium Layer

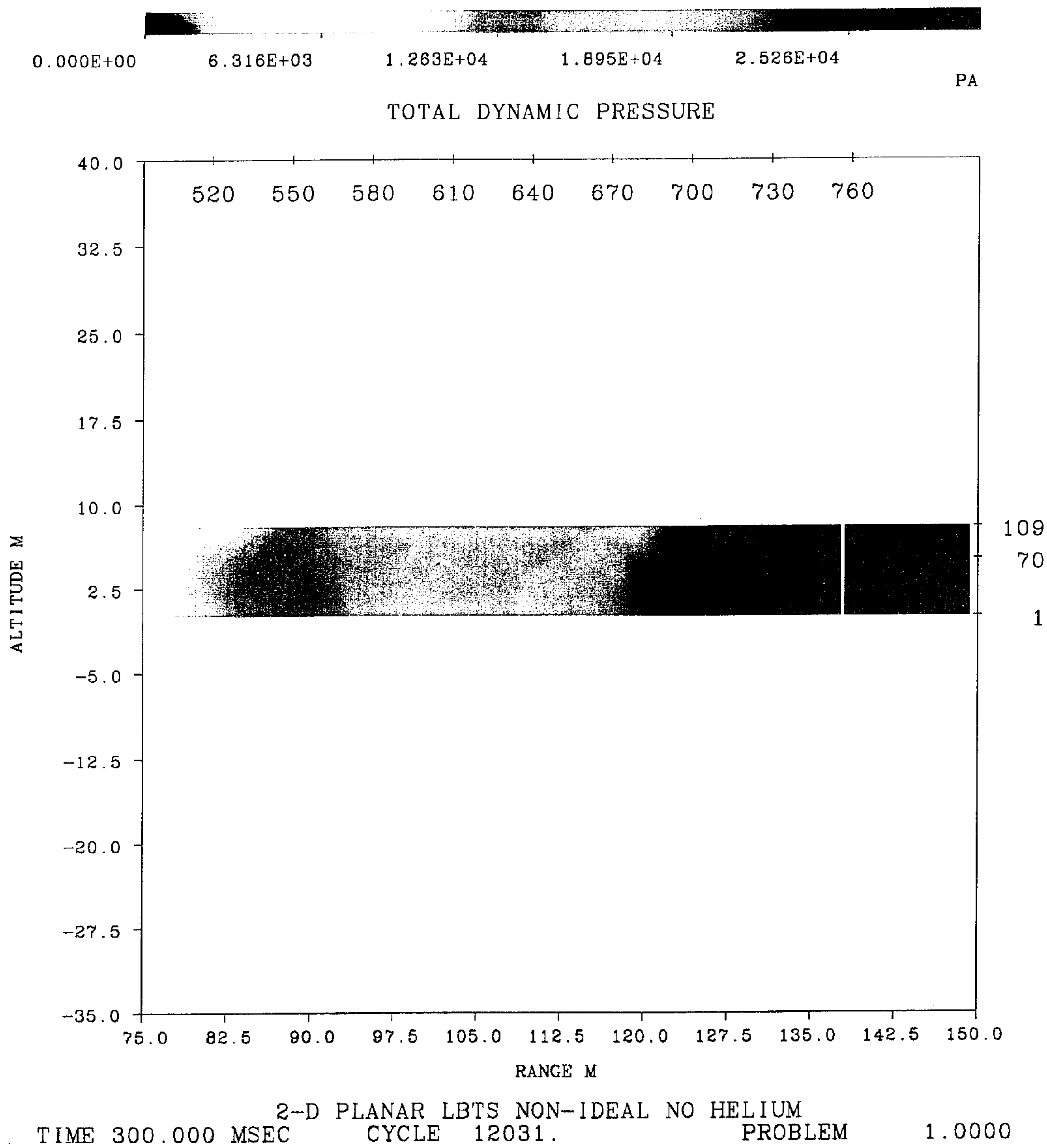

Figure 16. Dynamic Pressure in Expansion Section at 300 ms without Helium Layer

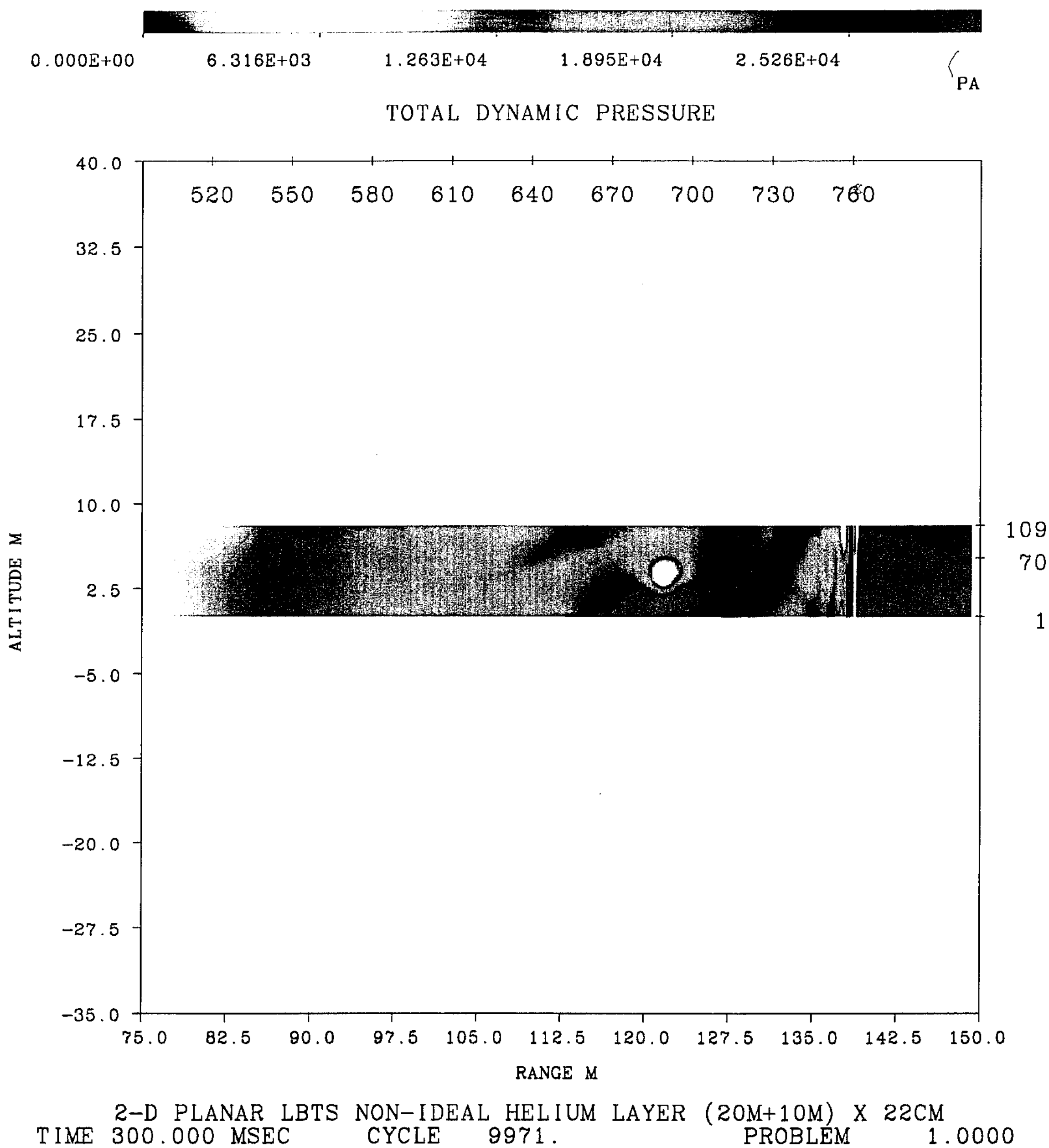

Figure 17. Dynamic Pressure in Expansion Section at 300 ms with Helium Layer

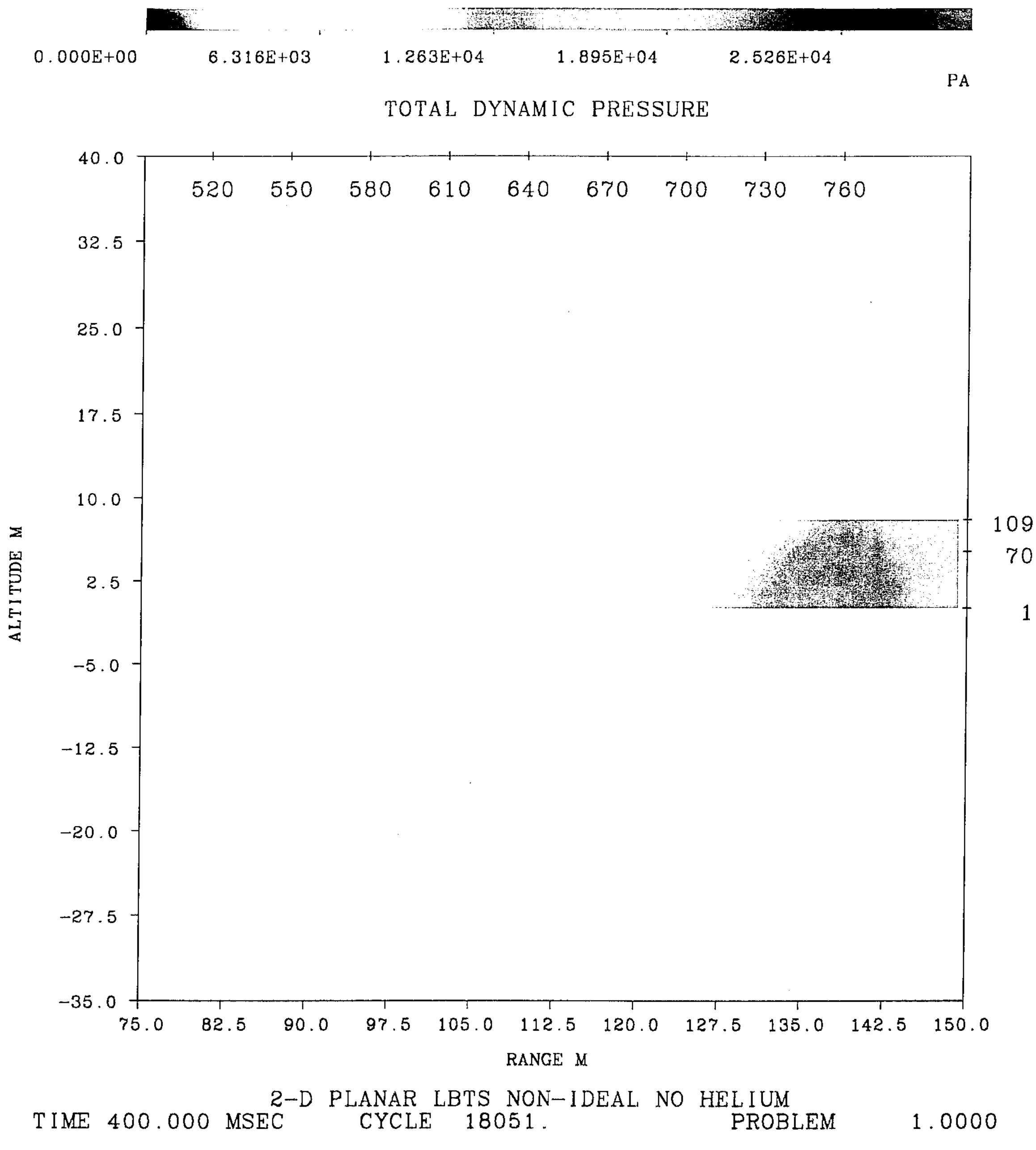

Figure 18. Dynamic Pressure in Expansion Section at 400 ms without Helium Layer

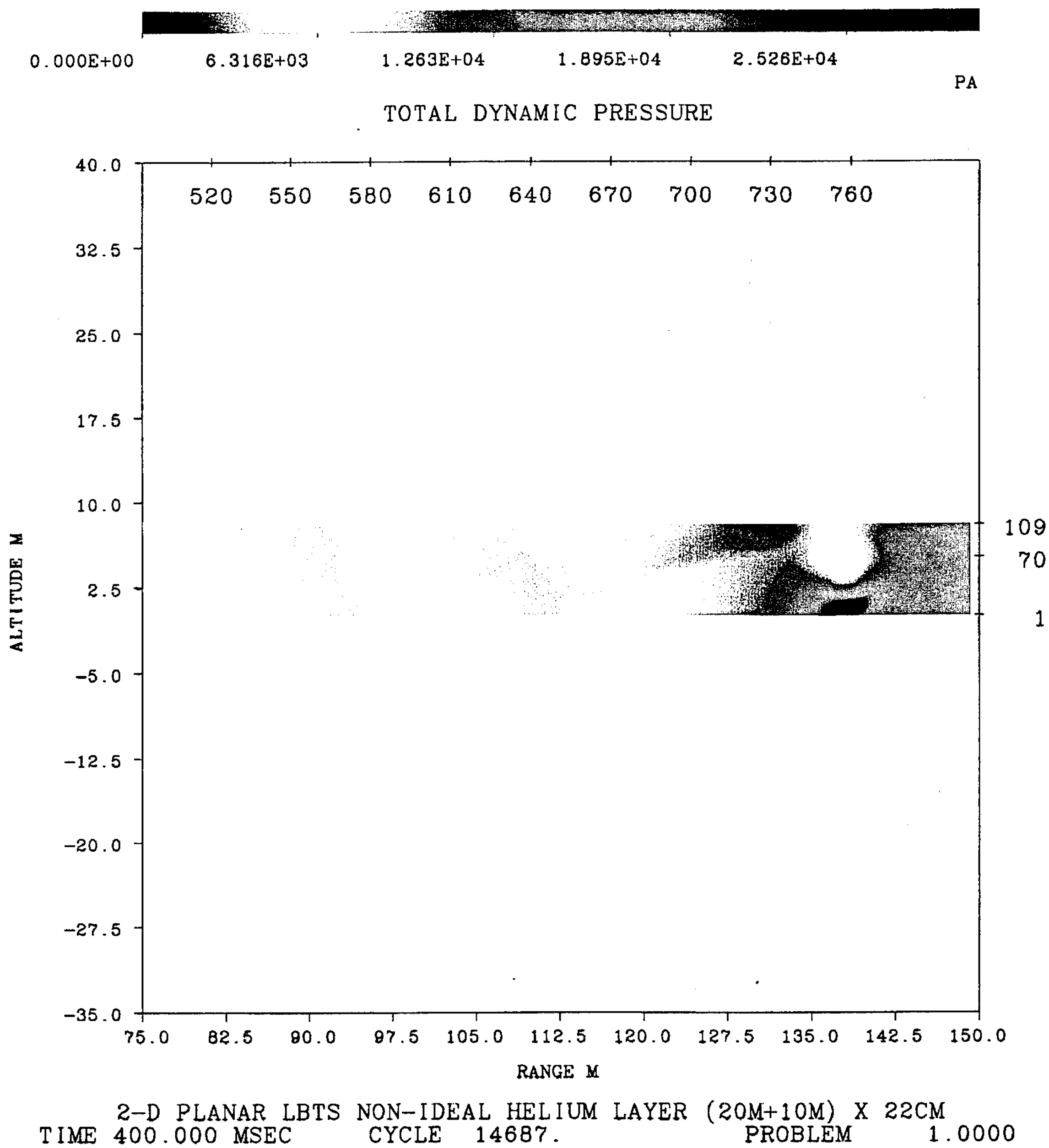

Figure 19. Dynamic Pressure in Expansion Section at 400 ms with Helium Layer

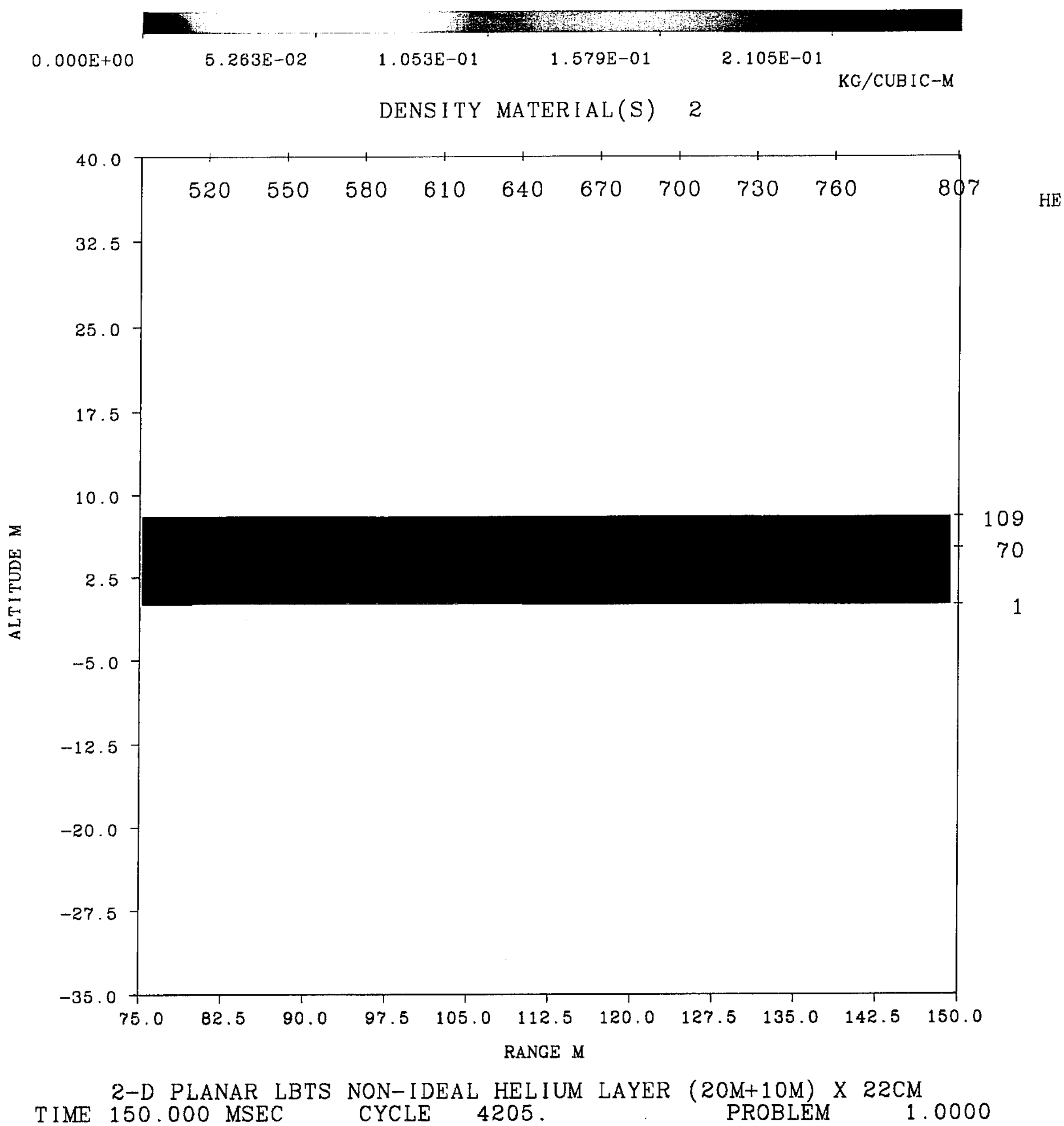

Figure 20. Helium Density in Expansion Section at 150 *ms*

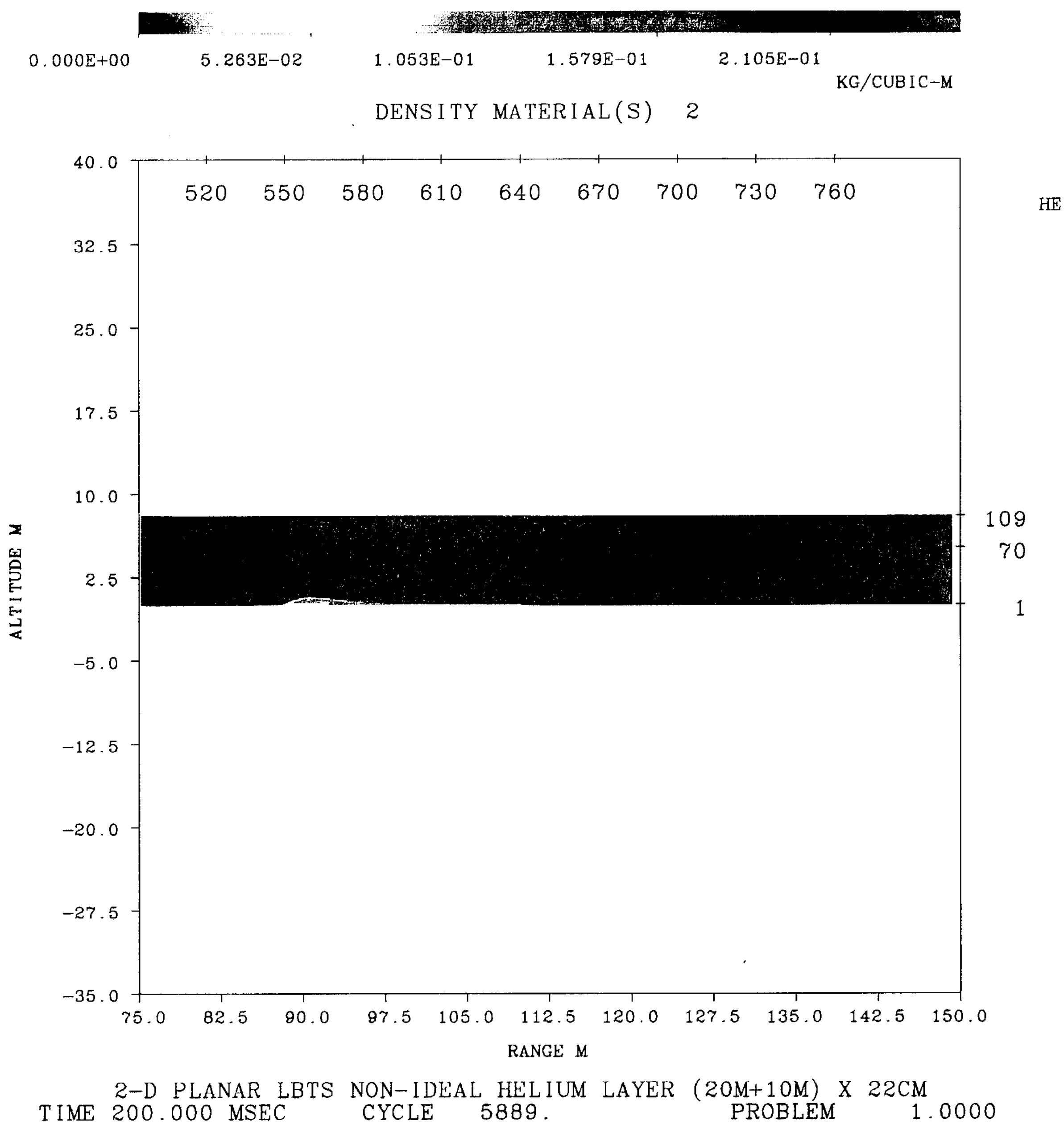

Figure 21. Helium Density in Expansion Section at 200 ms

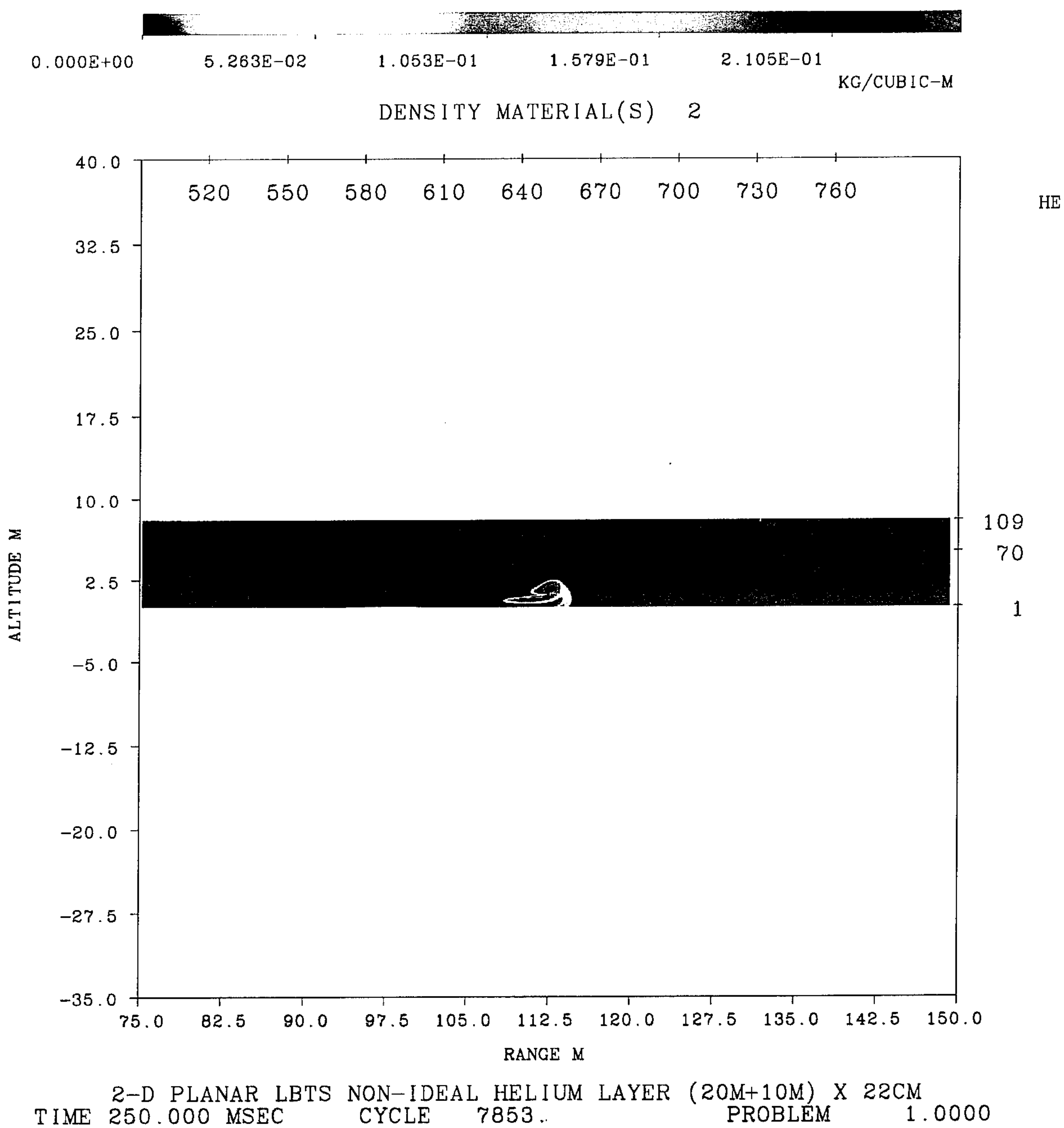

Figure 22. Helium Density in Expansion Section at 250 *ms*

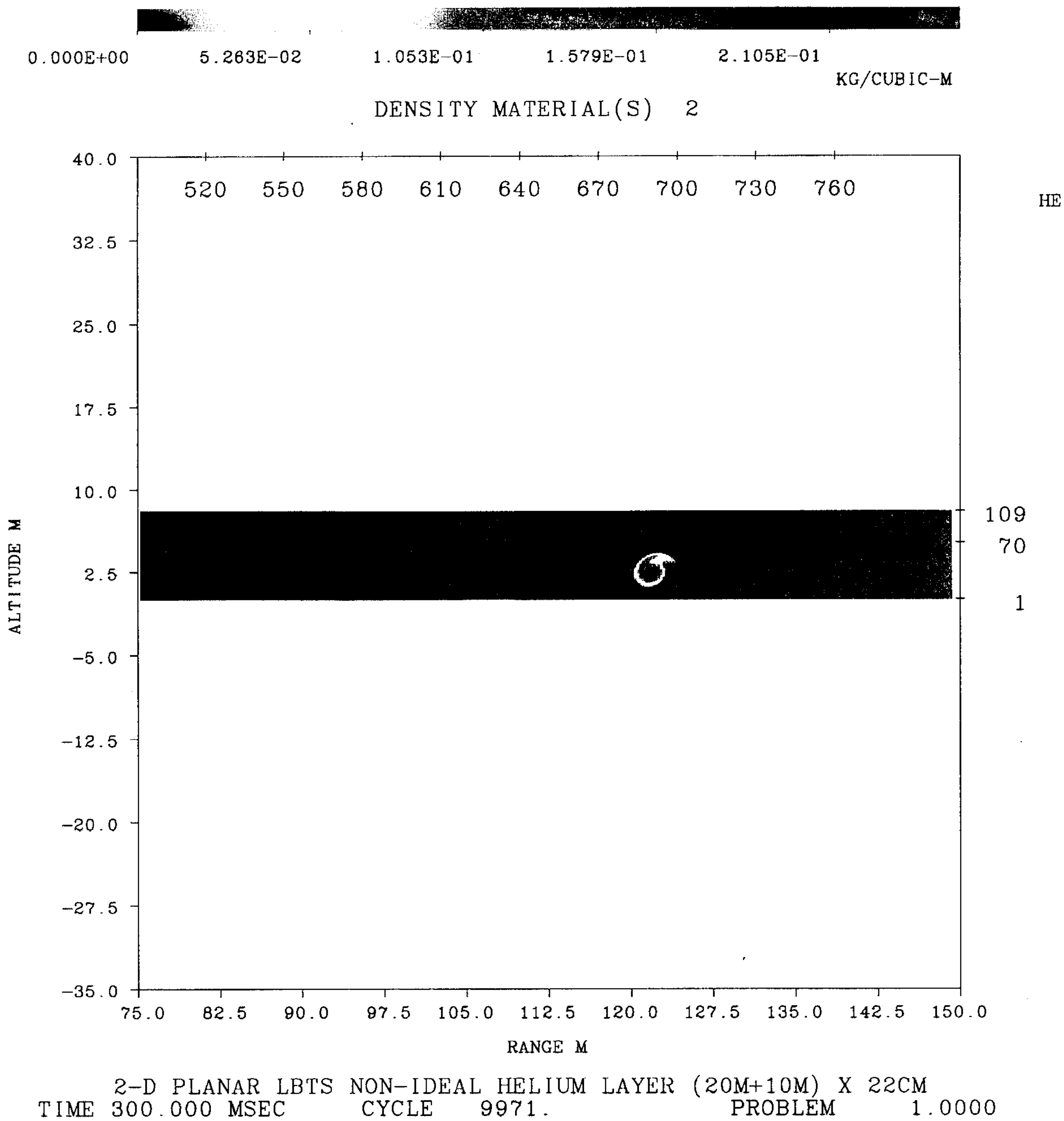

Figure 23. Helium Density in Expansion Section at 300 ms

Intentionally Left Blank

References

1. Glasstone, S. and P. Dolan - Editors. "The Effects of Nuclear Weapons." Department of Army Pamphlet No. 50-3, HQ, Department of Army. March 1977.

2. Liepmann H.W. and A. Roshko. "Elements of Gas Dynamics" John Wiley & Sons, Inc. 1957.

3. Kennedy, L. et al. - Editors "Capabilities of Nuclear Weapons, Chapter 2-Airblast Phenomena, Section 2II-Airblast Over Real Surfaces." DNA001-87-C-0141, Defense Nuclear Agency, Washington, DC. August 1988.

4. Needham, C., R. Ekler and L. Kennedy. "Extended Desert Calculation Results with Comparisons to PRISCILLA Experimental Data and a Near-Ideal Calculation." S-Cubed Report SSS-DTR-94-14802. September 1994.

5. Schraml, S. "Performance Predictions for the Large Blast/Thermal Simulator Based on Experimental and Computational Results." U.S. Army Ballistic Research Laboratory Technical Report BRL-TR-3232. Aberdeen Proving Ground, MD. May 1991.

6. Schraml, S. and R. Pearson. "Small Scale Shock Tube Experiments Using a Computer Controlled Active Rarefaction Wave Eliminator." U.S. Army Ballistic Research Laboratory Technical Report BRL-TR-3149. Aberdeen Proving Ground, MD. September 1990.

7. Reisler, R. et al. "DIAMOND ARC 87: Blast Phenomenology Results from HOB HE Tests with a Helium Layer." Aberdeen Research Center Report ARC-88-101. March 1988.

8. Hikida, S., R. Bell, and C. Needham. "The SHARC Codes: Documentation and Sample Problems." S-Cubed Technical Report SSS-R-89-9878. September 1988.

9. Barthel, J. "2-D Hydrocode Computations Using a $k - \epsilon$ Turbulence Model: Model Description and Test Calculations." S-Cubed Technical Report SSS-TR-85-7115. June 1985, (Footnotes added August 1988).

10. Schraml, S. "Characterization of Flow Distribution in Axisymmetric Shock Tubes." U.S. Army Ballistic Research Laboratory Technical Report BRL-TR-3353. Aberdeen Proving Ground, MD. June 1992.

11. Opalka, K. "Large Blast and Thermal Simulator Advanced Concept Driver Design by Computational Fluid Dynamics." U.S. Army Ballistic Research Laboratory Technical Report BRL-TR-3026. Aberdeen Proving Ground, MD. August 1989.

12. Martinez, E. Private Communication. February 1995.

13. Needham, C. et al. "Theoretical Calculation for Precursor Definition." DNA-TR-90-18, Defense Nuclear Agency, Washington, DC. September 1990.

Intentionally Left Blank

NO. OF COPIES	ORGANIZATION
2	ADMINISTRATOR ATTN DTIC DDA DEFENSE TECHNICAL INFO CTR CAMERON STATION ALEXANDRIA VA 22304-6145
1	DIRECTOR ATTN AMSRL OP SD TA US ARMY RESEARCH LAB 2800 POWDER MILL RD ADELPHI MD 20783-1145
3	DIRECTOR ATTN AMSRL OP SD TL US ARMY RESEARCH LAB 2800 POWDER MILL RD ADELPHI MD 20783-1145
1	DIRECTOR ATTN AMSRL OP SD TP US ARMY RESEARCH LAB 2800 POWDER MILL RD ADELPHI MD 20783-1145
	ABERDEEN PROVING GROUND
5	DIR USARL ATTN AMSRL OP AP L (305)

NO. OF COPIES	ORGANIZATION
2	HQDA ATTN SARD TR MS K KOMINOS DR R CHAIT PENTAGON WASHINGTON DC 20310-0103
1	HQDA ATTN SARD TT DR F MILTON PENTAGON WASHINGTON DC 20310-0103
2	DIRECTOR FEDERAL EMERGENCY MNGMNT AGENCY ATTN PUBLIC RELATIONS OFFICE TECHNICAL LIBRARY WASHINGTON DC 20472
1	CHAIRMAN DOD EXPLOSIVES SAFETY BOARD ROOM 856 C HOFFMAN BLDG 1 2461 EISENHOWER AVENUE ALEXANDRIA VA 22331-0600
1	DIRECTOR OF DEFENSE RESEARCH AND ENGINEERING ATTN DD TWP WASHINGTON DC 20301
1	DIRECTOR DEFENSE INTELLIGENCY AGENCY ATTN DT 2 WPNS & SYS DIVISION WASHINGTON DC 20301
1	ASSISTANT SECRETARY OF DEFENSE ATOMIC ENERGY ATTN DOCUMENT CONTROL WASHINGTON DC 20301
9	DIRECTOR DEFENSE NUCLEAR AGENCY ATTN CSTI TECHNICAL LIBRARY DDIR DFSP NANS OPNA SPSD SPTD DFTD TDTR WASHINGTON DC 20305

NO. OF COPIES	ORGANIZATION
1	CHAIRMAN JOINT CHIEFS OF STAFF ATTN J5 R&D DIVISION WASHINGTON DC 20301
2	DA DCSOPS ATTN TECHNICAL LIBRARY DIR OF CHEM & NUC OPS WASHINGTON DC 20310
3	COMMANDER FIELD COMMAND DNA ATTN FCPR FCTMOF NMHE KIRTLAND AFB NM 87115
1	U S ARMY RESEARCH DEVELOPMENT AND STANDARDIZATION GROUP UK ATTN DR ROY E REICHENBACH PSC 802 BOX 15 FPO AE 09499-1500
10	CENTRAL INTELLIGENCE AGENCY DIR DB STANDARD ATTN GE 47 HQ WASHINGTON DC 20505
1	DIRECTOR ADVANCED RESEARCH PROJECTS AGENCY ATTN TECHNICAL LIBRARY 3701 NORTH FAIRFAX DRIVE ARLINGTON VA 22203-1714
2	COMMANDER US ARMY NRDEC ATTN AMSNA D DR D SIELING STRNC UE J CALLIGEROS NATICK MA 01762
2	COMMANDER US ARMY CECOM ATTN AMSEL RD AMSEL RO TPPO P FT MONMOUTH NJ 07703-5301
1	COMMANDER US ARMY CECOM R&D TECHNICAL LIBRARY ATTN ASQNC ELC IS L R MYER CTR FT MONMOUTH NJ 07703-5000

NO. OF COPIES	ORGANIZATION
1	MIT ATTN TECHNICAL LIBRARY CAMBRIDGE MA 02139
1	COMMANDER US ARMY NGIC ATTN RESEARCH & DATA BRANCH 220 7TH STREET NE CHARLOTTESVILLE VA 22901-5396
1	COMMANDER US ARMY ARDEC ATTN SMCAR FSM W BARBER BLDG 94 PICATINNY ARSENAL NJ 07806-5000
1	DIRECTOR US ARMY TRAC FT LEE ATTN ATRC L MR CAMERON FT LEE VA 23801-6140
1	US ARMY MISSILE & SPACE INTELLIGENCE CENTER ATTN AIAMS YDL REDSTONE ARSENAL AL 35898-5500
1	COMMANDING OFFICER CODE L51 NAVAL CIVIL ENGINEERING LABORATORY ATTN J TANCRETO PORT HUENEME CA 93043-5003
2	COMMANDER US ARMY STRATEGIC DEFENSE COMMAND ATTN CSSD H MPL TECH LIB CSSD H XM DR DAVIES PO BOX 1500 HUNTSVILLE AL 35807
3	COMMANDER US ARMY CORPS OF ENGINEERS WATERWAYS EXPERIMENT STATION ATTN CEWES SS R J WATT CEWES SE R J INGRAM CEWES TL TECH LIBRARY PO BOX 631 VICKSBURG MS 39180-0631
1	COMMANDER US ARMY ENGINEER DIVISION ATTN HNDED FD PO BOX 1500 HUNTSVILLE AL 35807

NO. OF COPIES	ORGANIZATION
3	COMMANDER US ARMY NUCLEAR & CHEMICAL AGENCY 7150 HELLER LOOP SUITE 101 SPRINGFIELD VA 22150-3198
1	COMMANDER US ARMY CORPS OF ENGINEERS FT WORTH DISTRICT ATTN CESWF PM J PO BOX 17300 FT WORTH TEXAS 76102-0300
1	DIRECTOR TRAC FLVN ATTN ATRC FT LEAVENWORTH KS 66027-5200
1	COMMANDER US ARMY RESEARCH OFFICE ATTN SLCRO D PO BOX 12211 RESEARCH TRIANGLE PARK NC 27709-2211
1	COMMANDER NAVAL ELECTRONIC SYSTEMS COMMAND ATTN PME 117 21A WASHINGTON DC 20360
1	DIRECTOR HQ TRAC RPD ATTN ATRC RPR RADDA FT MONROE VA 23651-5143
2	OFFICE OF NAVAL RESEARCH ATTN DR A FAULSTICK CODE 23 800 N QUINCY STREET ARLINGTON VA 22217
1	DIRECTOR TRAC WSMR ATTN ATRC WC KIRBY WSMR NM 88002-5502
1	COMMANDER NAVAL SEA SYSTEMS COMMAND ATTN CODE SEA 62R DEPARTMENT OF THE NAVY WASHINGTON DC 20362-5101

NO. OF COPIES	ORGANIZATION
1	COMMANDER US ARMY WSMR ATTN STEWS NED DR MEASON WSMR NM 88002-5158
2	CHIEF OF NAVAL OPERATIONS DEPARTMENT OF THE NAVY ATTN OP 03EG OP 985F WASHINGTON DC 20350
1	COMMANDER DAVID TAYLOR RESEARCH CENTER ATTN CODE 522 TECH INFO CTR BETHESDA MD 20084-5000
1	OFFICER IN CHARGE CODE L31 CIVIL ENGINEERING LABORATORY NAVAL CONSTRUCTION BATTALION CTR ATTN TECHNICAL LIBRARY PORT HUENEME CA 93041
1	COMMANDING OFFICER WHITE OAK WARFARE CENTER ATTN CODE WA501 NNPO SILVER SPRING MD 20902-5000
1	COMMANDER CODE 533 NAVAL WEAPONS CENTER ATTN TECHNICAL LIBRARY CHINA LAKE CA 93555-6001
1	COMMANDER DAHLGREN DIVISION NAVAL SURFACE WARFARE CENTER ATTN CODE E23 LIBRARY DAHLGREN VA 22448-5000
1	COMMANDER NAVAL RESEARCH LABORATORY ATTN CODE 2027 TECHNICAL LIBRARY WASHINGTON DC 20375
1	OFFICER IN CHARGE WHITE OAK WARFARE CTR DETACHMENT ATTN CODE E232 TECHNICAL LIBRARY 10901 NEW HAMPSHIRE AVENUE SILVER SPRING MD 20903-5000
1	AL LSCF ATTN J LEVINE EDWARDS AFB CA 93523-5000

NO. OF COPIES	ORGANIZATION
1	COMMANDER NAVAL WEAPONS EVALUATION FAC ATTN DOCUMENT CONTROL KIRTLAND AFB NM 87117
1	RADC EMTLD DOCUMENT LIBRARY GRIFFISS AFB NY 13441
1	AEDC ATTN R MCAMIS MAIL STOP 980 ARNOLD AFB TN 37389
1	AFESC RDCS ATTN PAUL ROSENGREN TYNDALL AFB FL 32403
1	OLAC PL TSTL ATTN D SHIPLETT EDWARDS AFB CA 93523-5000
1	AFIT ENY ATTN LTC HASEN PHD WRIGHT PATTERSON AFB OH 45433-6583
2	AIR FORCE ARMAMENT LABORATORY ATTN AFATL DOIL AFATL DLYV EGLIN AFB FL 32542-5000
1	DIRECTOR IDAHO NATIONAL ENGINEERING LAB ATTN SPEC PROGRAMS J PATTON 2151 NORTH BLVD MS 2802 IDAHO FALLS ID 83415
3	PHILLIPS LABORATORY AFWL ATTN NTE NTED NTES KIRTLAND AFB NM 87117-6008
1	DIRECTOR LAWRENCE LIVERMORE NATIONAL LAB ATTN TECH INFO DEPT L 3 PO BOX 808 LIVERMORE CA 94550
1	AFIT ATTN TECHNICAL LIBRARY BLDG 640 B WRIGHT PATTERSON AFB OH 45433

NO. OF COPIES	ORGANIZATION
1	DIRECTOR NATIONAL AERONAUTICS & SPACE ADMIN ATTN SCIENTIFIC & TECH INFO FAC PO BOX 8757 BWI AIRPORT BALTIMORE MD 21240
1	FTD NIIS WRIGHT PATTERSON AFB OH 45433
3	KAMAN SCIENCES CORPORATION ATTN LIBRARY PA ELLIS FH SHELTON PO BOX 7463 COLORADO SPRINGS CO 80933-7463
4	DIRECTOR IDAHO NATIONAL ENGINEERING LAB EG&G IDAHO INC ATTN R GUENZLER MS 3505 R HOLMAN MS 3510 R A BERRY W C REED PO BOX 1625 IDAHO FALLS ID 83415
5	DIRECTOR SANDIA NATIONAL LABS ATTN DOC CONTROL 3141 C CAMERON DIV 6215 A CHABAI DIV 7112 D GARDNER DIV 1421 J MCGLAUN DIV 1541 PO BOX 5800 ALBUQUERQUE NM 87185-5800
2	DIRECTOR LOS ALAMOS NATIONAL LABORATORY ATTN TH DOWLER MS F602 DOC CONTROL FOR REPORTS LIBRARY PO BOX 1663 LOS ALAMOS NM 87545
1	BLACK & VEATCH ENGINEERS ARCHITECTS ATTN HD LAVERENTZ 1500 MEADOW LAKE PARKWAY KANSAS CITY MO 64114

NO. OF COPIES	ORGANIZATION
1	DIRECTOR SANDIA NATIONAL LABORATORIES LIVERMORE LABORATORY ATTN DOC CONTROL FOR TECH LIB PO BOX 969 LIVERMORE CA 94550
1	DIRECTOR NASA AMES RESEARCH CENTER APPLIED COMPUTATIONAL AERO BRANCH ATTN DR T HOLTZ MS 202 14 MOFFETT FIELD CA 94035
1	DIRECTOR NASA LANGLEY RESEARCH CENTER ATTN TECHNICAL LIBRARY HAMPTON VA 23665
2	APPLIED RESEARCH ASSOCIATES INC ATTN J KEEFER NH ETHRIDGE PO BOX 548 ABERDEEN MD 21001
1	ADA TECHNOLOGIES INC ATTN JAMES R BUTZ HONEYWELL CENTER SUITE 110 304 INVERNESS WAY SOUTH ENGLEWOOD CO 80112
1	ALLIANT TECHSYSTEMS INC ATTN ROGER A RAUSCH MN48 3700 7225 NORTHLAND DRIVE BROOKLYN PARK MN 55428
1	CARPENTER RESEARCH CORPORATION ATTN H JERRY CARPENTER 27520 HAWTHORNE BLVD SUITE 263 PO BOX 2490 ROLLING HILLS ESTATES CA 90274
1	AEROSPACE CORPORATION ATTN TECH INFO SERVICES PO BOX 92957 LOS ANGELES CA 90009
1	GOODYEAR CORPORATION ATTN RM BROWN BLDG 1 SHELTER ENGINEERING LITCHFIELD PARK AZ 85340

NO. OF COPIES	ORGANIZATION
1	THE BOEING COMPANY ATTN AEROSPACE LIBRARY PO BOX 3707 SEATTLE WA 98124
2	FMC CORPORATION ADVANCED SYSTEMS CENTER ATTN J DROTLEFF C KREBS MDP 95 BOX 58123 2890 DE LA CRUZ BLVD SANTA CLARA CA 95052
1	CALIFORNIA RES & TECH INC ATTN M ROSENBLATT 20943 DEVONSHIRE STREET CHATSWORTH CA 91311
1	SVERDRUP TECHNOLOGY INC SVERDRUP CORPORATION AEDC ATTN BD HEIKKINEN MS 900 ARNOLD AFB TN 37389-9998
2	DYNAMICS TECHNOLOGY INC ATTN D T HOVE G P MASON 21311 HAWTHORNE BLVD SUITE 300 TORRANCE CA 90503
1	KTECH CORPORATION ATTN DR E GAFFNEY 901 PENNSYLVANIA AVE NE ALBUQUERQUE NM 87111
1	EATON CORPORATION DEFENSE VALVE & ACTUATOR DIV ATTN J WADA 2338 ALASKA AVE EL SEGUNDO CA 90245-4896
2	MCDONNELL DOUGLAS ASTRONAUTICS CORP ATTN ROBERT W HALPRIN KA HEINLY 5301 BOLSA AVENUE HUNTINGTON BEACH CA 92647

NO. OF COPIES	ORGANIZATION
4	KAMAN AVIDYNE ATTN R RUETENIK 2 CP S CRISCIONE R MILLIGAN 83 SECOND AVENUE NORTHWEST INDUSTRIAL PARK BURLINGTON MA 01830
1	MDA ENGINEERING INC ATTN DR DALE ANDERSON 500 EAST BORDER STREET SUITE 401 ARLINGTON TX 07601
2	PHYSICS INTERNATIONAL CORPORATION PO BOX 5010 SAN LEANDRO CA 94577-0599
2	KAMAN SCIENCES CORPORATION ATTN DASIAC PO DRAWER 1479 816 STATE STREET SANTA BARBARA CA 93102-1479
1	R&D ASSOCIATES ATTN GP GANONG PO BOX 9377 ALBUQUERQUE NM 87119
1	LOCKHEED MISSILES & SPACE CO ATTN J J MURPHY DEPT 81 11 BLDG 154 PO BOX 504 SUNNYVALE CA 94086
2	SCIENCE CENTER ROCKWELL INTERNATIONAL CORP ATTN DR S CHAKRAVARTHY DR D OTA 1049 CAMINO DOS RIOS THOUSAND OAKS CA 91358
1	ORLANDO TECHNOLOGY INC ATTN D MATUSKA 60 SECOND STREET BLDG 5 SHALIMAR FL 32579

NO. OF COPIES	ORGANIZATION
3	S CUBED A DIVISION OF MAXWELL LABS INC ATTN TECHNICAL LIBRARY R DUFF K PYATT PO BOX 1620 LA JOLLA CA 92037-1620
2	THE RALPH M PARSONS COMPANY ATTN T M JACKSON LB TS PROJECT MANAGER 100 WEST WALNUT STREET PASADENA CA 91124
1	SAIC ATTN J GUEST 2301 YALE BLVD SE SUITE E ALBUQUERQUE NM 87106
1	SUNBURST RECOVERY INC ATTN DR C YOUNG PO BOX 2129 STEAMBOAT SPRINGS CO 80477
1	SAIC ATTN N SINHA 501 OFFICE CENTER DRIVE APT 420 FT WASHINGTON PA 19034-3211
1	SVERDRUP TECHNOLOGY INC ATTN RF STARR PO BOX 884 TULLAHOMA TN 37388
2	S CUBED A DIVISION OF MAXWELL LABS INC ATTN C E NEEDHAM L KENNEDY 2501 YALE BLVD SE ALBUQUERQUE NM 87106
3	SRI INTERNATIONAL ATTN DR GR ABRAHAMSON DR J GRAN DR B HOLMES 333 RAVENWOOD AVENUE MENLO PARK CA 94025

NO. OF COPIES	ORGANIZATION
1	TRW BALLISTIC MISSILE DIVISION ATTN H KORMAN MAIL STATION 526 614 PO BOX 1310 SAN BERNADINO CA 92402
1	BATTELLE TWSTIAC 505 KING AVENUE COLUMBUS OH 43201-2693
1	THERMAL SCIENCE INC ATTN R FELDMAN 2200 CASSENS DRIVE ST LOUIS MO 63026
2	DENVER RESEARCH INSTITUTE ATTN J WISOTSKI TECHNICAL LIBRARY PO BOX 10758 DENVER CO 80210
1	STATE UNIVERSITY OF NEW YORK MECHANICAL & AEROSPACE ENGINEERING ATTN DR PEYMAN GIVI BUFFALO NY 14260
2	UNIVERSITY OF MARYLAND INSTITUTE FOR ADV COMPUTER STUDIES ATTN L DAVIS G SOBIESKI COLLEGE PARK MD 20742
2	THINKING MACHINES CORPORATION ATTN G SABOT R FERREL 245 FIRST STREET CAMBRIDGE MA 02142-1264
1	NORTHROP UNIVERSITY ATTN DR FB SAFFORD 5800 W ARBOR VITAE STREET LOS ANGELES CA 90045
1	CALIFORNIA INSTITUTE OF TECHNOLOGY ATTN T J AHRENS 1201 E CALIFORNIA BLVD PASADENA CA 91109

NO. OF COPIES	ORGANIZATION
1	STANFORD UNIVERSITY ATTN DR D BERSHADER DURAND LABORATORY STANFORD CA 94305
1	UNIVERSITY OF MINNESOTA ARMY HIGH PERF COMP RES CTR ATTN DR TAYFUN E TEZDUYAR 1100 WASHINGTON AVE SOUTH MINNEAPOLIS MN 55415
3	SOUTHWEST RESEARCH INSTITUTE ATTN DR C ANDERSON S MULLIN A B WENZEL PO DRAWER 28255 SAN ANTONIO TX 78228-0255
2	COMMANDER US ARMY NRDEC ATTN SSCNC YSD J ROACH SSCNC WST A MURPHY KANSAS STREET NATICK MA 10760-5018

NO. OF COPIES	ORGANIZATION
	ABERDEEN PROVING GROUND
1	CDR USATECOM ATTN AMSTE TE F L TELETSKI
1	CDR USATHAMA ATTN AMSTH TE
1	CDR USATC ATTN STEC LI
26	DIR USARL ATTN AMSRL SC C H BREAUX AMSRL SC CC C NIETUBICZ C ELLIS D HISLEY N PATEL T KENDALL R SHEROKE AMSRL SC I W STUREK AMSRL SC AE M COLEMAN AMSRL SC S R PEARSON AMSRL SL CM E FIORVANTE AMSRL WT N J INGRAM AMSRL WT NA R KEHS AMSRL WT NC R LOTTERO B MCGUIRE A MIHALCIN P MULLER R LOUCKS S SCHRAML AMSRL WT ND J MILETTA AMSRL WT NF L JASPER AMSRL WT NG T OLDHAM AMSRL WT NH J CORRIGAN AMSRL WT PB P WEIHNACHT B GUIDOS AMSRL WT TC K KIMSEY

USER EVALUATION SHEET/CHANGE OF ADDRESS

This Laboratory undertakes a continuing effort to improve the quality of the reports it publishes. Your comments/answers to the items/questions below will aid us in our efforts.

1. ARL Report Number ARL-TR-869 Date of Report September 1995

2. Date Report Received ______________________________

3. Does this report satisfy a need? (Comment on purpose, related project, or other area of interest for which the report will be used.) ______________________________

4. Specifically, how is the report being used? (Information source, design data, procedure, source of ideas, etc.) ______________________________

5. Has the information in this report led to any quantitative savings as far as man-hours or dollars saved, operating costs avoided, or efficiencies achieved, etc? If so, please elaborate. ______________________________

6. General Comments. What do you think should be changed to improve future reports? (Indicate changes to organization, technical content, format, etc.) ______________________________

CURRENT ADDRESS

Organization

Name

Street or P.O. Box No.

City, State, Zip Code

7. If indicating a Change of Address or Address Correction, please provide the Current or Correct address above and the Old or Incorrect address below.

OLD ADDRESS

Organization

Name

Street or P.O. Box No.

City, State, Zip Code

(Remove this sheet, fold as indicated, tape closed, and mail.)

(DO NOT STAPLE)

DEPARTMENT OF THE ARMY

OFFICIAL BUSINESS

NO POSTAGE NECESSARY IF MAILED IN THE UNITED STATES

BUSINESS REPLY MAIL

FIRST CLASS PERMIT NO 0001,APG,MD

POSTAGE WILL BE PAID BY ADDRESSEE

DIRECTOR
U.S. ARMY RESEARCH LABORATORY
ATTN: AMSRL-WT-NC
ABERDEEN PROVING GROUND, MD 21005-5066